Ahmed Abdalla, 2025, 13:3
ISSN (Online): 2348-4098
ISSN (Print): 2395-4752

International Journal of Science,
Engineering and Technology

An Open Access Journal

Design Of Horizontal Axis Wind Turbine (HAWT)

[1]Ahmed Tarek El-Sayed, [1]Ahmed Mahmoud Makram ,[1]Ahmed Mamdouh Mohamed,
[1]Eslam Mohamed Waheed , [1]Eslam Mohamed Yehia, [2]Dr. Mostafa Shawky Abdelmoez
[1]Scholar Mechanical Power Engineering, Cairo University
[2]Lecturer, Mechanical Power dept. Faculty of Engineering, Cairo University, Supervisor

Abstract- Cairo University, Faculty of Engineering This research presents a detailed investigation into the design of a Horizontal Axis Wind Turbine (HAWT) blade, applying advanced methodologies such as Exergy Analysis, Fatigue Analysis, and Damping Analysis. The design process began with the development of the blade geometry using optimized performance equations, followed by the use of the Blade Element Momentum (BEM) method. This method effectively integrates the principles of blade element theory with momentum theory to provide an accurate representation of aerodynamic forces. After the design was completed, Exergy Analysis was conducted to evaluate the thermodynamic performance and efficiency of the system. The Fatigue Analysis was carried out to assess the blade's resistance to cyclic stresses over its operational life. Additionally, Damping Analysis was performed to study the stability and vibrational characteristics of the blade, ensuring its long-term functionality. The findings aim to contribute to the development of more efficient and sustainable wind turbine technologies.

Keywords- Wind Turbine Blade Design, Horizontal Axis Wind Turbine (HAWT), Blade Element Momentum Theory (BEM), Aerodynamic Optimization, Structural Analysis, Exergy Analysis, Fatigue Analysis, Damping Characteristics, Renewable Energy Systems, Thermodynamic Efficiency, Performance Modeling, Sustainable Energy Design, Rotor Dynamics, Mechanical Integrity

I. INTRODUCTION

The increasing global demand for energy, coupled with the environmental consequences of fossil fuel dependency, has accelerated the shift toward renewable energy sources. Wind energy, in particular, has emerged as a leading solution for clean and sustainable electricity generation. Horizontal Axis Wind Turbines (HAWTs) have proven to be highly efficient and compatible with large-scale power systems, making them a top choice in many wind energy projects.

The rotor is one of the most critical components of a wind turbine, as it converts wind energy into mechanical energy. Therefore, the aerodynamic and structural design of the rotor blades is essential for achieving optimal performance. In designing efficient blades, analytical methods such as Actuator Disc Theory, General Momentum Theory, and Blade Element Momentum (BEM) Theory are commonly used. These models help predict airflow behavior and performance characteristics, considering factors like tip loss and axial induction correction.

The aerodynamic forces acting on the blades, such as lift, drag, and thrust, are fundamental to turbine operation. The proper distribution of these forces is crucial to maximize energy capture while minimizing structural stress and fatigue. The selection of airfoils and the blade geometry - including chord length, twist angle, and tapering - are tailored based on aerodynamic flow conditions and the targeted operating range.

Additionally, the blade design must account for dynamic forces resulting from varying wind speeds and turbulent conditions.

The design process also incorporates damping effects, which are essential for stabilizing rotor motion and reducing vibrations that could lead to fatigue over time. Various damping mechanisms - such as structural damping, aerodynamic damping, and hydrodynamic damping - contribute to the overall dynamic behavior of the turbine. Aerodynamic damping, in particular, results from the interaction between the rotor blades and the wind. This damping helps reduce unwanted vibrations, especially in larger turbines where aeroelastic effects become more pronounced. The impact of aerodynamic damping on blade stability and fatigue loading is crucial for ensuring the turbine's durability throughout its operational life.

Meteorological factors, such as temperature, humidity, and air pressure, also affect the aerodynamic performance of the turbine. For example, variations in air density can influence the amount of energy the rotor captures. These environmental variables must be integrated into both theoretical models and practical design considerations to ensure optimal performance under various operational conditions. Thermodynamic principles, including Exergy Analysis, are used to evaluate system performance beyond traditional efficiency metrics, as this analysis examines irreversibilities and entropy generation within the system, providing a deeper understanding of energy losses under varying environmental conditions.

Recent advancements in simulation techniques, such as Computational Fluid Dynamics (CFD), have significantly improved the accuracy of aerodynamic predictions, enabling detailed modeling of airflow around turbine blades. While CFD is a powerful tool, as noted, we will not be utilizing it in this study. Instead, our approach will rely on a combination of experimental data, semi-empirical models, and stress analysis using software like SolidWorks to evaluate the structural behavior of the blades under operational conditions, including dynamic forces from wind gusts, turbulence, and pitch variations.

In this study, a wind turbine rotor is analyzed using BEM theory, with a focus on the impact of meteorological parameters across different wind speeds and pitch angles. Additionally, stress analysis is conducted on the designed blade to evaluate its structural integrity under varying aerodynamic forces and operational loads. This comprehensive approach, combining aerodynamic modeling, thermodynamic evaluation, damping effects, and mechanical simulation, aims to enhance both the performance and durability of wind turbine blades, ensuring they can withstand the dynamic loading conditions they face in real-world environments.

II. LITERATURE REVIEW

Evolution of Wind Power Technology and the Emergence of Horizontal-Axis Wind Turbines (HAWTs):

The harnessing of wind energy dates back to ancient times, where early civilizations employed basic windpowered devices for mechanical tasks such as grain milling and water lifting. One of the earliest known applications appeared in Persia around the 7th century, featuring vertical-axis windmills with simple, rectangular blades mounted on vertical shafts.

During the Middle Ages, wind energy utilization spread across Europe, particularly in regions like the Netherlands, where horizontal-axis windmills became prominent in land drainage and agricultural processing. These early systems marked a significant advancement in wind harnessing efficiency and mechanical design.

The industrial revolution ushered in a new era for wind energy with attempts to convert wind power into electricity. In the late 19th century, several experimental wind turbines were constructed for domestic lighting, particularly in remote areas lacking grid infrastructure. As technological understanding progressed, larger prototypes emerged in the U.S. and Europe, although they faced challenges related to cost and reliability.

Figure 1: Early Wind Turbines Nashtifan wind turbines in Sistan, Iran

By the early 20th century, electrically-generating wind turbines began appearing in utility-scale experiments. A notable early example was a 100 kW horizontal-axis wind turbine installed in the USSR during the 1930s, which was directly connected to a local grid. In the 1940s, the U.S. introduced the first megawatt-scale wind turbine; however, it was short-lived due to wartime resource limitations.

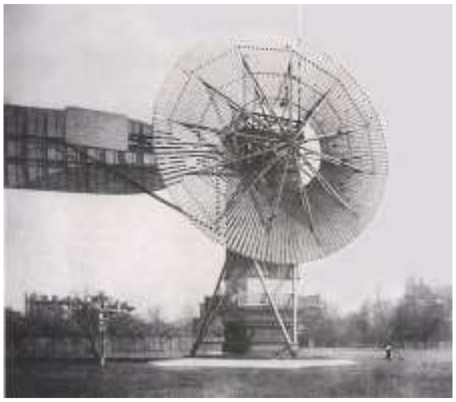

Figure 2: The first automatically operated wind turbine, built in Cleveland in 1887 by Charles F. Brush

The modern shift towards wind energy began in the 1970s, fueled by oil crises and growing environmental awareness. Denmark played a leading role through grassroots engineering efforts, which resulted in the development of highly efficient small turbines. Over time, these evolved into larger, grid-compatible machines, with significant support from cooperative models, policy frameworks, and international collaborations.

- Why Horizontal-Axis Wind Turbines?

Horizontal-Axis Wind Turbines (HAWTs) gained prominence due to their superior efficiency in converting wind energy into electrical power. Their aerodynamic design—where blades rotate perpendicular to the wind—maximizes lift and minimizes drag, enhancing overall performance. HAWTs are particularly effective in open, high-wind environments and are easier to scale for utility-level energy production. In addition to higher energy yields, HAWTs offer structural and operational advantages. Their orientation allows for better yaw control and more consistent performance. Their costeffectiveness, durability, and compatibility with large systems have made them the top choice for commercial wind power.

III. METHODOLOGY (THEORIES)

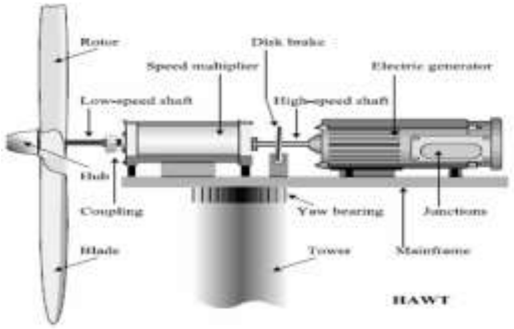

Figure 3: Main Components of HAWT

Wind turbine power generation depends on aerodynamic blade-wind interactions that convert kinetic energy into electricity, with efficiency determined by blade design and operating conditions. This research integrates multiple aerodynamic and structural theories to enhance accuracy and reliability. These include:

The Actuator Disc Theory and The Betz Limit:
The actuator disk model (Betz, 1926) provides fundamental wind turbine aerodynamics analysis by treating the rotor as a homogeneous disk that creates a pressure discontinuity in the wind flow. This idealized approach assumes steady, incompressible flow with infinite blades, no rotation in wake, and uniform thrust distribution. The model calculates maximum extractable power (Betz limit), thrust forces, and wake effects using control volume analysis, forming the basis for all wind turbine aerodynamic theories.

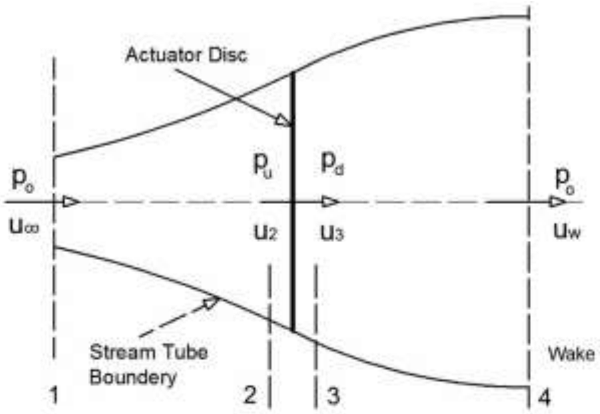

Figure 4: flow through a wind turbine flow through a wind turbine by a non-rotating actuator disc

From continuity:

$$u_2 = u_3 = u_R$$

For steady state flow:

$$\dot{m} = \rho A u_R$$

Thrust on the wind turbine is caused by the change in momentum of the air as it flows through the rotor:

$$T = -\dot{m}(u_\infty - u_w)$$

From Bernoulli:

$$p_o + \frac{1}{2}\rho u_\infty^2 = p_u + \frac{1}{2}\rho u_R^2$$

$$p_d + \frac{1}{2}\rho u_R^2 = p_o + \frac{1}{2}\rho u_w^2$$

Thrust as the net sum forces on disk sides:

$$T = Ap'$$

where,

$$p' = (p_u - p_d)$$

then,

$$p' = \frac{1}{2}\rho(u_\infty^2 - u_w^2)$$

$$T = \frac{1}{2}\rho A(u_\infty^2 - u_w^2)$$

Matching thrust equations gives the rotor velocity:

$$u_R = \frac{u_\infty + u_w}{2}$$

The axial induction factor (a) measures how much the wind slows down at the rotor. then,

$$a = \frac{u_\infty - u_R}{u_\infty}$$

$$u_R = u_\infty(1-a)$$

So,

$$u_w = u_\infty(1-2a)$$

As air passes through the rotor, it slows down and the flow area expands due to continuity. A sudden pressure drop at the rotor plane generates the torque needed to rotate the turbine blades.

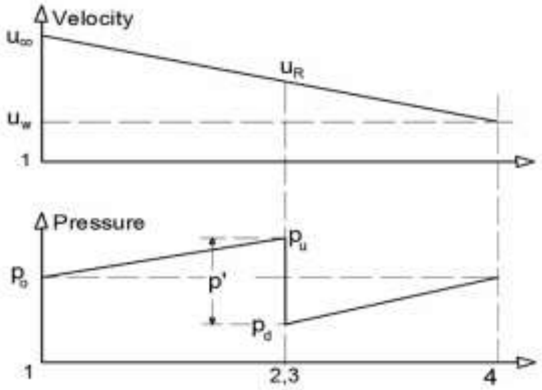

Figure 5: Velocity and Pressure distribution along the stream tube

Power output:

$$P = Tu_R$$

Substituting by torque:

$$P = \frac{1}{2}\rho A(u_\infty^2 - u_w^2)u_R$$

Then substitute by velocities,

$$P = 2\rho Aa(1-a)^2 u_\infty^3$$

Wind turbine performance is evaluated using the power coefficient (C_p), a dimensionless number that expresses how efficiently the turbine converts wind energy into mechanical power.

$$C_P = \frac{P}{0.5\rho u_\infty^3 A}$$

Substituting by the power. Then,

$$C_p = 4a(1-a)^2$$

Taking the derivative to evaluate the maximum C_p:

$$(C_p)_{max} = \frac{16}{27} = 0.5926$$

At a=1/3 , the turbine reaches the Betz limit (its maximum power output). The axial thrust can then be calculated by:

$$T = 2\rho Aa(1-a)u_\infty^2$$

Similar to power coefficient, the thrust coefficient is the thrust force divided by the wind's dynamic force.

$$C_T = \frac{T}{0.5\rho u_\infty^2 A}$$

$$C_T = 4a(1-a)$$

Substituting the torque:

The optimum value of Cp can be reached by setting the differentiation of Cp to zero,

$$\frac{dC_P}{da} = 4(1-a)(1-3a) = 0$$

The optimum value of Cp can be reached by setting the differentiation of Cp to zero,

(optimum value of 16/27 at a=1/3)

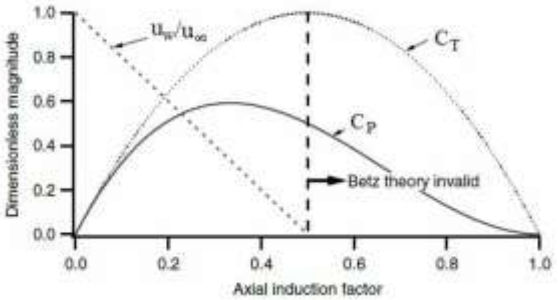

Figure 6: Operating parameters for a Betz turbine

The General Momentum Theory

The wind turbine rotor slows the wind and extracts energy by creating a pressure drop across the rotor. When extended to include rotation, the theory accounts for the torque exerted by the rotor, which causes the wake to spin in the opposite direction. This rotational wake carries away energy, reducing efficiency especially in slow, high-torque turbines. So, while basic momentum theory assumes no rotation, the full picture includes angular momentum and wake losses.

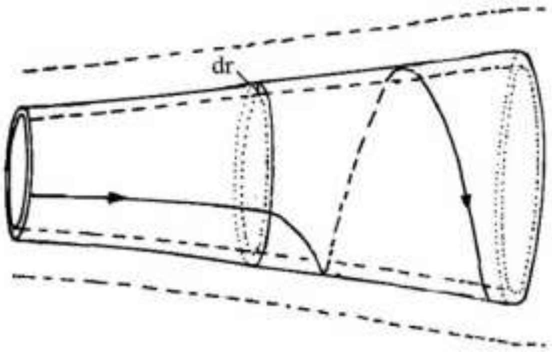

Figure 7: Stream tube model of flow behind rotating wind turbine blade

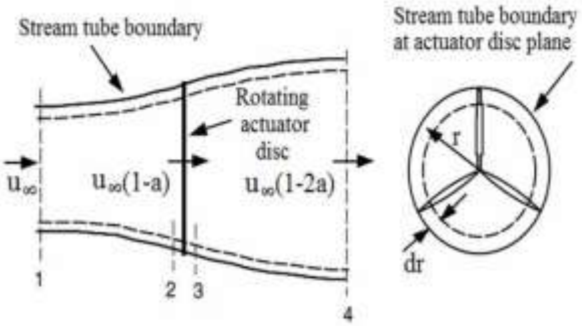

Figure 8: Geometry for rotor analysis

In a rotating control volume, the energy equation shows that the pressure difference across the blades is linked to changes in the air's angular velocity from Ω to $\Omega+\omega$ while the axial velocity stays the same. This helps explain how blades generate torque and affect pressure.

$$p_2 - p_3 = \rho\left(\Omega + \frac{1}{2}\omega\right)\omega r^2$$

The Resulting Thrust dT:

$$dT = 4a'(1+a')\frac{1}{2}\rho\Omega^2 r^2 \, 2\pi r dr$$

The angular induction factor, denoted as a′, defined as:

$$a' = \omega / 2\Omega$$

When wake rotation is considered, the induced velocity at the rotor includes both the axial component u_∞ and a rotational component $r\Omega a'$.

$$dT = (p_2 - p_3)dA = \left[\rho\left(\Omega + \frac{1}{2}\omega\right)\omega r^2\right]2\pi r dr$$

Then the thrust expression is: Using the previous linear momentum analysis, the thrust on an annular cross-section is determined by the axial induction factor a, with the free-stream velocity u1 represented as u_∞, Then the thrust expression is:

$$dT = 4a(1-a)\frac{1}{2}\rho u_\infty^2 \, 2\pi r dr$$

Equating the two equations of thrust:

$$\frac{a(1-a)}{a'(1+a')} = \frac{\Omega^2 r^2}{u_\infty^2} = \lambda_r^2$$

Where,

λr is the local tip speed ratio defined as the ratio of the blade tip speed to the free stream wind speed:

$$\lambda = \Omega R / u_\infty$$

The tip speed ratio at a specific radius (intermediate radius):

$$\lambda_r = \Omega r / u_\infty = \lambda r / R$$

The torque on the rotor Q is derived using the conservation of angular momentum. It equals the change in angular momentum of the wake, which can be expressed for an incremental annular area element as:

$$dQ = d\dot{m}(\omega r)(r) = (\rho u_2 2\pi r dr)(\omega r)(r)$$

Since,

$$u_2 = u_\infty(1-a) \quad \text{and} \quad a' = \omega/2\Omega$$

Then,

$$dQ = 4a'(1-a)\frac{1}{2}u_\infty \Omega r^2 2\pi r dr$$

The power generated at each element, dP, is given by:

$$dP = \Omega dQ$$

Substituting for dQ in this expression and using the definition of the local speed ratio, λr, then the expression for the power generated at each element becomes:

$$dP = \frac{1}{2}\rho A u_\infty^3\left[\frac{8}{\lambda^2}a'(1-a)\lambda_r^3 d\lambda_r\right]$$

Power from each annular ring depends on the axial and angular induction factors and the tip speed ratio. These factors shape airflow at the rotor and influence local power contribution. So, the incremental contribution to the power coefficient, dCp, from each annular ring is given by:

$$dC_P = \frac{dP}{1/2\rho A u_\infty^3}$$

Then,

$$C_P = \frac{8}{\lambda^2}\int_0^\lambda a'(1-a)\lambda_r^3 d\lambda_r$$

Relating the variables a, a', and λr, we get:

$$a' = -\frac{1}{2} + \frac{1}{2}\sqrt{\left[1 + \frac{4}{\lambda_r^2}a(1-a)\right]}$$

Maximum power is achieved when the term a′(1−a) is maximized. By substituting a′ and setting the derivative with respect to a to zero, the optimal conditions for power extraction are found. Then,

$$\lambda_r^2 = \frac{(1-a)(4a-1)^2}{1-3a}$$

So, for maximum power in each annular ring:

$$a' = \frac{1-3a}{4a-1}$$

Taking the differentiation with respect to a:

$$2\lambda_r d\lambda_r = \left[6(4a-1)(1-2a)^2/(1-3a)^2\right]$$

Substituting in the maximum power coefficient equation:

$$C_{P,\max} = \frac{24}{\lambda^2}\int_{a_1}^{a_2}\left[\frac{(1-a)(1-2a)(1-4a)}{(1-3a)}\right]^2 da$$

Here the lower limit of integration, a1, corresponds to the axial induction factor for λr= λh=0 and the upper limit, a2, corresponds to the axial induction factor at λr=λ.

So,

$$\lambda^2 = (1-a_2)(1-4a_2)/(1-3a_2)$$

Equation analysis shows that a1=0.25 leads to a tip speed ratio of zero, while a2=1/3 is the theoretical upper limit for a, giving an infinite tip speed ratio. To solve the integral, a variable substitution simplifies the expression and leads to:

$$C_{P,\max} = \frac{8}{729\lambda^2}\left\{\begin{array}{c}\frac{64}{5}x^5 + 72x^4 + 124x^3 \\ +38x^2 - 63x \\ -12\ln x - 4x^{-1}\end{array}\right\}_{x=(1-3a_2)}^{x=0.25}$$

Figure 9 shows that as the tip-speed ratio increases, the maximum power coefficient also increases. It compares results from general momentum theory with the Betz limit and links each power coefficient to its corresponding axial induction factor at the blade tip.

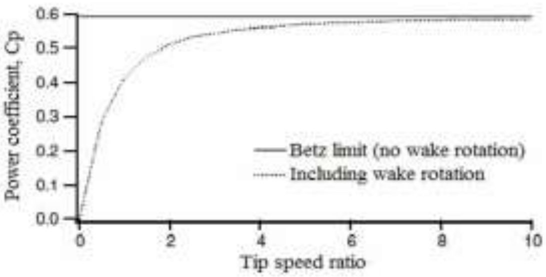

Figure 9: Theoretical maximum power coefficient as a function of tip speed ratio for an ideal HAWT with and without wake rotation.

Momentum theory with wake rotation

The conservation of angular momentum in an annular stream tube is used in momentum theory to analyze rotor behavior. The thrust on a small element is calculated using axial momentum theory as follows:

$$dT = 2\rho u\left(u - U_\infty\right)dA = 4\pi\rho U_\infty^2 a(1-a)rdr$$

Introducing wake rotation and employing the angular momentum theory, the thrust force on the element is given by:

$$dT = 4\pi\rho\Omega^2 a'\left(1+a'\right)r^3 dr$$

where r is the radius of the differential element of thickness dr. a′ is the tangential induction, or interference, factor defined as:

$$a' = \frac{\omega}{2\Omega}$$

where, Ω is the rotor angular speed. ω is the wake angular velocity.

Figure 8 shows that the airflow has no rotation before the blades but gains rotational speed ω\omegaω in the wake. The average tangential velocity at the blade is based on inlet and exit conditions.

$$\Omega r + \frac{1}{2}\omega r = \Omega r\left(1 - a'\right)$$

Using this, expressions are derived for:

- Torque on a differential element: depends on air density, wind speed, induction factors, and radius.

$$dQ = 4\pi\rho U_\infty \Omega a'(1-a)r^3 dr$$

- Power on a differential element: derived from torque and related to the tip speed ratio λ and local speed ratio λr.

$$dP = \Omega dQ = \frac{1}{2}\rho A U_\infty^3 \frac{8}{\lambda^2} a'(1-a)\lambda_r^3 d\lambda_r$$

- Speed ratios: λr is the local ratio at radius r, and λ is the overall tip speed ratio using rotor radius R, they are expressed by:

$$\lambda_r = \frac{\Omega r}{U_\infty}$$

$$\lambda = \frac{\Omega R}{U_\infty}$$

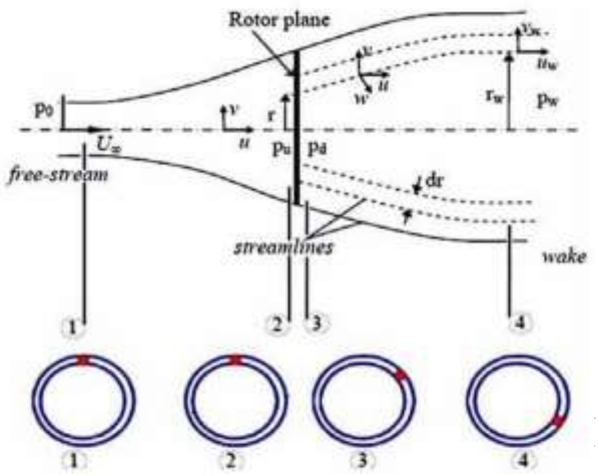

reduction. While these methods provide the theoretical maximum power coefficient relative to wind speed and power extracted, they don’t account for detailed rotor geometry, such as airfoil shape, chord length, or blade twist.

To address this limitation, blade element theory is used. In this method, the blade is conceptually divided into multiple sections, and each section is analyzed individually. Aerodynamic forces are calculated using airfoil data for each cross-section, summing the forces from all elements.

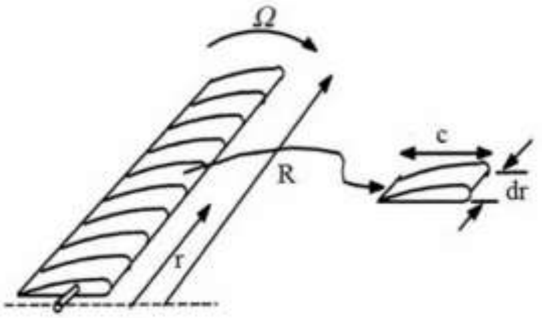

Figure 11: Schematic of blade elements

Figure 12 shows the forces and velocities acting on a blade element at radius r. The relative wind velocity urel is the result of two components:

- The axial component, u∞(1−a), accounts for the freestream wind reduced by axial induction.
- The rotational component, Ωr(1+a′), combines blade rotation and induced angular velocity.

The diagram helps explain how wind slows down approaching the rotor and how wake rotation contributes to torque generation.

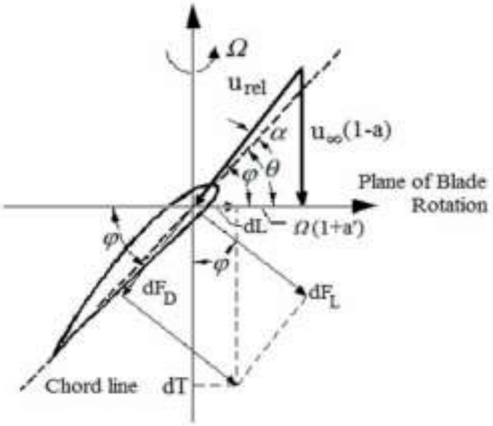

Figure 12: Blade geometry for analysis of a HAWT

From the velocity diagram in Fig.10, the following relationships can be determined:

$$\varphi = \theta + \alpha$$

$$u_{rel} = \frac{u_\infty(1-a)}{\sin(\varphi)}$$

$$\tan(\varphi) = \frac{u_\infty(1-a)}{\Omega r(1+a')} = \frac{(1-a)}{(1+a')\lambda_r}$$

$$dF_D = C_D \frac{1}{2}\rho u_{rel}^2 c dr$$

$$dF_L = C_L \frac{1}{2}\rho u_{rel}^2 c dr$$

$$dT = dF_L\cos(\varphi) + dF_D\sin(\varphi)$$

$$dL = dF_L\sin(\varphi) - dF_D\cos(\varphi)$$

Considering the number of blades B, the total normal (trust) and tangential force on the element at a distance r calculated as the following:

$$dT = B\frac{1}{2}\rho u_{rel}^2(C_L\cos(\varphi) + C_D\sin(\varphi))cdr$$

$$dL = B\frac{1}{2}\rho u_{rel}^2(C_L\sin(\varphi) - C_D\cos(\varphi))cdr$$

The elemental torque due to the tangential forces, dL operating at a distance r from the center is given by:

$$dQ = rdL$$

Then,

$$dQ = B\frac{1}{2}\rho u_{rel}^2(C_L\sin(\varphi) - C_D\cos(\varphi))crdr$$

Defining the solidity ratio σ by:

$$\sigma = \frac{Bc}{2\pi r}$$

By substitution, the general form of elemental thrust, and torque equations become:

$$dT = \sigma\pi\rho\frac{u_\infty{}^2(1-a)^2}{\sin^2(\phi)}(C_L\cos(\phi) + C_D\sin(\phi))rdr$$

$$dQ = \sigma\pi\rho\frac{u_\infty{}^2(1-a)^2}{\sin^2(\phi)}(C_L\sin(\phi) - C_D\cos(\phi))r^2dr$$

Blade element theory leads to the previous two key equations that express thrust and torque on a rotor section based on flow angles and airfoil properties. This theory relies on two main assumptions:

- Each blade element acts independently of its neighbors.
- The airfoil data used matches the shape and behavior of each element.

Blade Element-momentum (BEM)Theory

Momentum theory focuses on angular momentum conservation within an annular stream tube, introducing wake rotation - a component that absents in the simpler actuator disk approach, which only accounts for axial flow and thus cannot model torque. However, momentum theory does not account for rotor geometry, such as blade chord, twist, or blade count.

In contrast, blade element theory analyzes the aerodynamic forces acting on individual blade sections, providing expressions for thrust and power similar to those in momentum theory. When combined, the two methods form the Blade Element Momentum (BEM) theory, which is widely used to evaluate wind turbine blade performance.

While BEM theory is relatively simple and gives reasonably accurate results, it has limitations. It doesn’t fully capture certain aerodynamic effects, such as high induction levels in heavily loaded rotors, hub and tip losses, or skewed flow when the rotor isn't aligned with the wind. In such cases, correction models are typically applied.

Equating dT for both blade element theory and momentum theory with wake rotation:

$$\frac{a}{1-a} = \sigma C_L \frac{\cos\phi}{4\sin^2\phi}\left[1 + \left(\frac{C_D}{C_L}\right)\tan\phi\right]$$

And by substituting by a′ formula got in the momentum theory with wake rotation we get:

$$\frac{a'}{1-a}=\frac{\sigma C_L}{4\lambda_r \sin\phi}\left[1-\left(\frac{C_D}{C_L}\right)\cot\phi\right]$$

The glide ratio (CL/CD) is typically maximized at the design angle of attack to ensure maximum torque from the blade element. Since CL is much larger than CD, CD is often neglected in related equations.

From velocity triangles:

$$\tan\phi=\frac{1-a}{(1+a')\lambda_r}$$

Substituting and rearranging:

$$\frac{a'}{1\mp a'}=\frac{\sigma C_L}{4\cos\phi}\left[1-\left(\frac{C_D}{C_L}\right)\cot\phi\right]$$

Since CD/CL is much less than 1, CD is set to zero, simplifying equations:

$$\frac{a}{1-a}=\sigma C_L\frac{\cos\phi}{4\sin^2\phi}$$

$$\frac{a'}{1-a}=\frac{\sigma C_L}{4\lambda_r \sin\phi}$$

$$\frac{a'}{1+a}=\frac{\sigma C_L}{4\cos\phi}$$

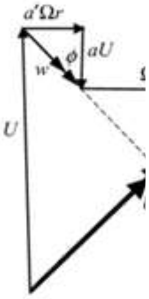

Figure 13: Velocity triangle for the flow over a blade element showing the relative velocity of the flow with respect to the blade element

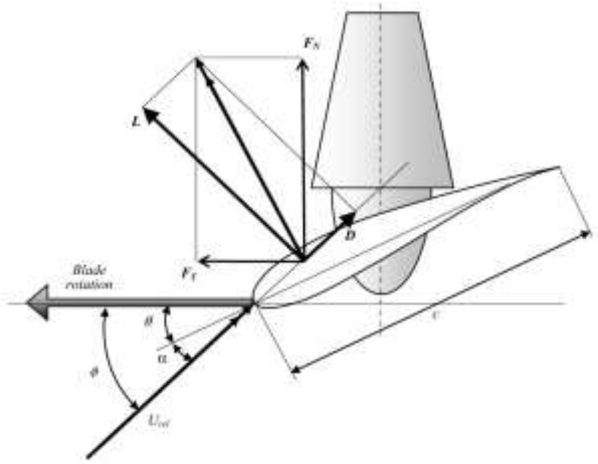

Figure 14: Aerodynamic forces on a blade element

Solving for a and a′:

$$a=\frac{1}{1+\frac{4\sin^2\phi}{\sigma C_n}}$$

$$a'=\frac{1}{\frac{4\sin\phi\cos\phi}{\sigma C_t}-1}$$

The normal and tangential force coefficients are given by:

$$C_n=C_L\cos\phi+C_D\sin\phi$$

$$C_t=C_L\sin\phi-C_D\cos\phi$$

Setting CD equals zero,

$$a=\frac{1}{1+\frac{4\sin^2\phi}{\sigma C_L\cos\phi}}$$

$$a'=\frac{1}{\frac{4\cos\phi}{\sigma C_L}-1}$$

Using relationships from the velocity triangle, it's shown that cotangent of the product of axial induction and local speed ratio equals the flow angle. This relation, combined with other expressions, allows the lift coefficient to be defined based on the local speed ratio, flow angle, and element solidity:

$$C_L=\frac{4\sin\phi(\cos\phi-\lambda_r\sin\phi)}{\sigma(\sin\phi+\lambda_r\cos\phi)}$$

The output power from each element is calculated by:

$$dP = \Omega dQ$$

$$P = \int_{r_h}^{R} \Omega dQ$$

where, r_h is the hub radius. Then,

$$C_P = \frac{P}{P_{wind}} = \frac{\int_{r_h}^{R} \Omega dQ}{\frac{1}{2}\rho\pi U_\infty^3 R^2}$$

perform integration:

$$C_P = \frac{8}{\lambda^2}\int_{\lambda_h}^{\lambda} \lambda_r^3 a'(1-a)\left[1-\frac{C_D}{D_L}\cot\phi\right] d\lambda_r$$

Dividing total length from hub to tip into n elements:

$$C_P = \frac{8}{\lambda}\frac{R-r_h}{nR}\sum_{i=1}^{n} F\lambda_r^3 a'(1-a)\left(1-\frac{C_D}{C_L}\cot\phi\right)$$

Or,

$$C_P = \frac{8}{\lambda n}\sum_{i=1}^{n} F\sin^2\phi\left(\cos\phi-\lambda_r\sin\phi\right)$$

$$\left(\sin\phi+\lambda_r\cos\phi-\frac{C_D}{C_L}\cot\phi\right)\lambda_r^2$$

where, F is loss factor.

when, CD ≈ 0, the equation above for C_p is the same as the one derived from the general momentum theory. An alternative expression for the power coefficient can be derived after performing the tedious algebra:

Note that even though the axial and angular induction factors were determined assuming the CD=0, the drag is included in the power coefficient calculation. By the same token, the thrust coefficient CT can be found beginning from the definition of thrust coefficient as follows:

$$C_P = \frac{8}{\lambda^2}\int_{\lambda_h}^{\lambda}\left[\begin{array}{l}\sin^2(\phi)(\cos(\phi)-\lambda_r\sin(\phi))(\sin(\phi)\\ +\lambda_r\cos(\phi))\left[1-(C_D/C_L)\cot(\phi)\right]\lambda_r^2\end{array}\right] d\lambda_r$$

$$C_T = \frac{4}{\lambda^2}\int_{\lambda_h}^{\lambda}\left[\begin{array}{l}\sin^2(\phi)(\cos(\phi)-\lambda_r\sin(\phi))(\sin(\phi)\\ +\lambda_r\cos(\phi))\left[1+(C_D/C_L)\cot(\phi)\right]\lambda_r^2\end{array}\right] d\lambda_r$$

IV. THEORY-DRIVEN DESIGN

This chapter covers the application of Blade Element Momentum (BEM) theory in designing HAWT blades and analyzing rotor performance. It includes tip-loss factors, flow states, airfoil selection criteria, and outlines the blade design and power prediction procedures. Various methods for HAWT blade design and performance prediction are also reviewed.

The Tip-Loss Factor

Previous theories assumed an infinite number of blades, neglecting radial flow across the rotor. However, near the blade tips, air flows around the edges due to pressure differences, creating radial velocity. This tip flow reduces lift and power near the blade tips.

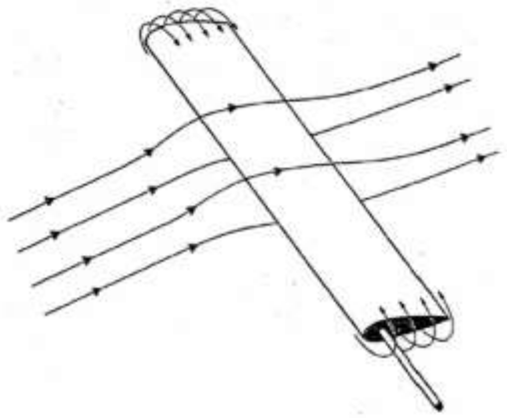

Figure 15: Tip loss flow diagram

According to Glauert theory, an optimum blade has uniform circulation, shedding vorticity only at the root and tip. Prandtl's model describes the rotor wake as a helical vortex sheet, and the tip-loss factor accounts for radial flow effects near the blade tip. His method provides a good approximation, especially for turbines with high tip speed ratios and two or more blades.

$$F_{tip} = \frac{2}{\pi}\cos^{-1}\exp\left(-\frac{B(1-r/R)}{2(r/R)\sin\phi}\right)$$

The tip loss factor decreases towards zero at the tip. In addition, the hub loss factor is given by:

$$F_{hub} = \frac{2}{\pi}\cos^{-1}\exp\left(-\frac{B(r-r_{hub})}{2r\sin\phi}\right)$$

Then, the total loss factor equals:

$$F = F_{tip}.F_{hub}$$

The expressions for axial (a) and tangential (a′) induction factors, incorporating tip-loss correction and neglecting drag, are used in the analysis.

$$a = \frac{1}{1 + \dfrac{4F\sin^2\phi}{\sigma C_L \cos\phi}}$$

$$a' = \frac{1}{\dfrac{4F\cos\phi}{\sigma C_L} - 1}$$

Then, the equation of CL including loss factor is given by

$$C_L = \frac{4F\sin\phi\left(\cos\phi - \lambda_r \sin\phi\right)}{\sigma\left(\sin\phi + \lambda_r \cos\phi\right)}$$

Notice that the flow angle φ can be calculated from:

$$\phi = \tan^{-1}\left(\frac{a'\lambda_r}{a}\right)$$

and,

$$C_P = \frac{8}{\lambda^2}\int_{\lambda_h}^{\lambda}\left[\begin{array}{l} F\sin^2(\phi)(\cos(\phi) - \lambda_r\sin(\phi))(\sin(\phi) \\ +\lambda_r\cos(\phi))\left[1-(C_D/C_L)\cot(\phi)\right]\lambda_r^2 \end{array}\right] d$$

5.2 Axial induction factor correction

Based on the momentum theory assumptions, the velocity in the far wake, denoted as Vw, can be determined as follows:

$$V_w = U_\infty(1-2a)$$

When the axial induction factor a reaches 0.5, the wake velocity becomes zero,

causing the momentum theory to fail, as streamlines no longer exist. Thrust continues to increase beyond this point, even reaching CT = 2.0 for a > 0.5. The BEM theory accurately predicts the axial induction factor for values of a < 0.4, while at high winds, a turbulent wake state with turbulence and recirculation forms behind the rotor.

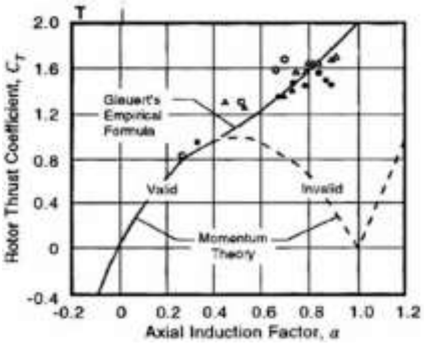

Figure 16: Relationship between axial induction, flow state and thrust of rotor

Buhl's equation for a:

In regions where momentum theory breaks down, empirical relationships between the thrust coefficient (CT) and the axial induction factor (a) are commonly

$$a = \frac{18F - 20 - 3\sqrt{C_T(50-36F) + 12F(3F-4)}}{36F - 50}$$

to a great extent then

Wilson-Walker method:

applied to correct their values. These corrections are typically integrated into the iterative process used to compute both a and a′. The following section outlines widely used correction methods for axial induction.

a. Glauert method:

Glauert method is employed for a > 0.4 or equivalently CT > 0.96. Glauert's empirical equation is given by:

$$a = \frac{1}{F}\left[0.143 + \sqrt{0.0203 - 0.6427(0.889 - C_T)}\right]$$

F is Prandtl's tip loss factor and CT is calculated from:

$$C_T = \frac{F\sigma(1-a)^2 C_n}{\sin^2\phi}$$

b. Buhl method:

The following relation for the thrust coefficient for CT > 0.96 is given by:

$$C_T = \frac{8}{9} + \left(4F - \frac{40}{9}\right)a + \left(\frac{50}{9} - 4F\right)a^2$$

methods. However, no results are reported in literature for the application of Spera correction in the analysis of turbine blade performance. Most of the work done used Buhl Glauert and Wilson-Walker corrections. c. Wilson-Walker method:

Figure 17: Axial induction factor correction methods for different

Above a value of a = 0.2, Wilson-Walker method may be

$$C_T = \begin{cases} 4a(1-a)F & a \le a_c \\ 4\left(a_c^2+(1-2a_c)a\right)F & a > a_c \end{cases}$$

$$a=\frac{1}{2}\Big[2+K(1-2a_c) - \sqrt{\left(K(1-2a_c)+2\right)^2+4\left(Ka_c^2-1\right)}\Big]$$

where,

d. Spera's method: Spera introduced a straightforward empirical formula that defines the axial induction factor (a) as a function of the thrust coefficient across its entire range. This relation offers a practical approach for modeling a throughout all operating conditions.

$$K=\frac{4F\sin^2\phi}{\sigma C_n}$$

$$a=\frac{1}{F}(0.27C$$

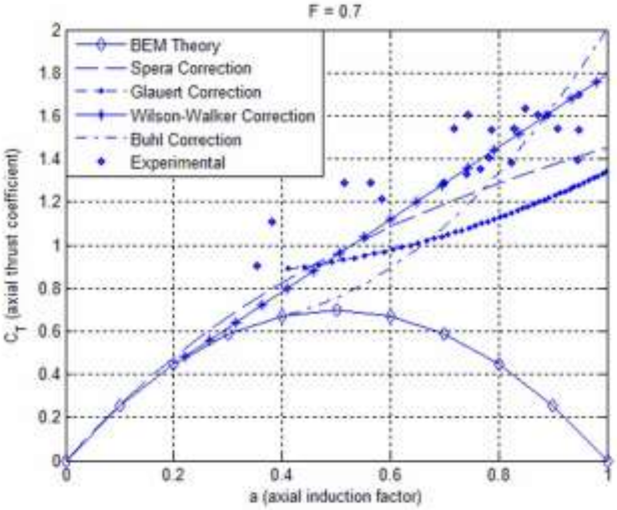

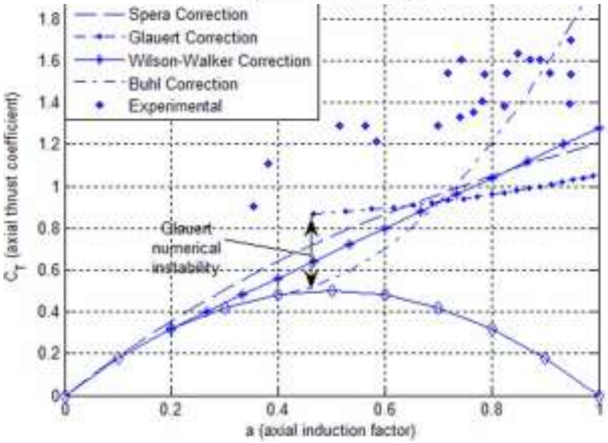

Then,

The axial induction factor is reliably predicted only within the range of 0.0 to 0.4; beyond that, BEM theory loses accuracy. Glauert's correction is valid only when the tip-loss factor equals 1. For lower values of the tip-loss factor, Buhl and WilsonWalker corrections offer more accurate and stable results. These methods also address numerical instabilities that arise with Glauert's correction when tip losses are present. It is shown that Glauert's method does not maintain continuity for tip-loss factors less than It can be inferred that Spera correction seems to better match the experimental results than the other

$$C_P=\frac{8}{\lambda^2}\int_{\lambda_h}^{\lambda} F\lambda_r^3 a'(1-a)\left[1-\frac{C_D}{D_L}\cot\phi\right]d\lambda_r$$

HAWT Flow States:

axial induction factors, wind turbine performance well with Blade Element Momentum (BEM) However, when the axial induction factor ; 0.5, general momentum theory fails, as it ately predicts negative wake velocities. In reality, v becomes complex, entering what's known as ulent wake state.

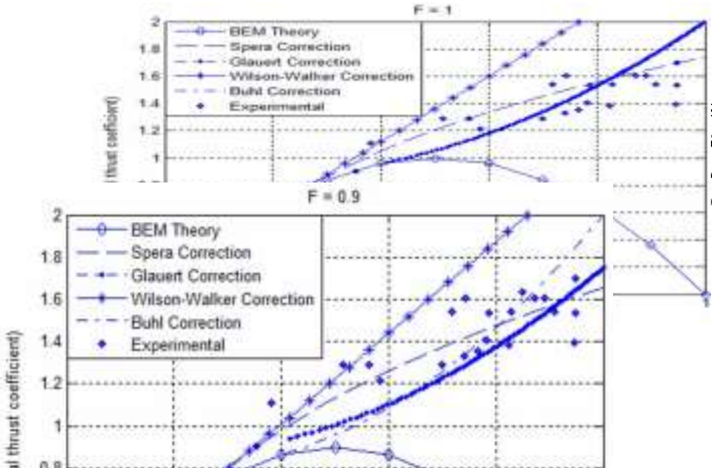

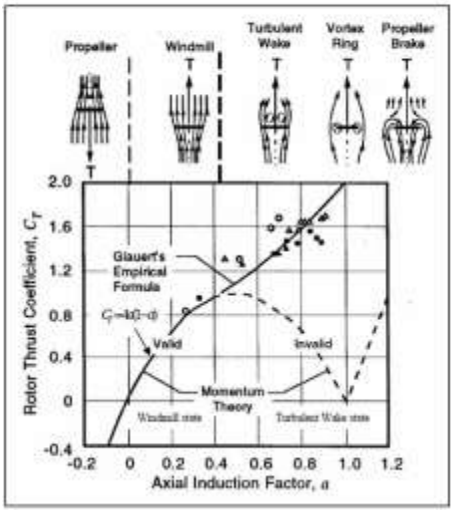

Figure 18: Relationship between axial induction, flow state and thrust of a rotor Key flow states:

- Propeller state: For negative induction factors (a < 0), the turbine behaves like a propeller, adding energy to the flow (CT < 0).
- Windmill state: Normal operating mode for HAWTs, valid for a < 0.5, where general momentum theory holds.
- Turbulent wake state: Occurs when a > 0.5, where thrust increases with induction factor (up to ~2), contrary to theoretical predictions.
- Vortex ring state: Begins when a > 1, indicating even more complex flow.
- Propeller brake state: When a > 2.0, flow reverses direction, and the rotor generates downwind thrust by adding power to the flow.

Due to the limitations of general momentum theory at higher induction factors, Glauert's empirical formula is used (especially for 0.4 < a < 1.0), in combination with blade element theory and accounting for tip losses, to better model rotor behavior in these complex states.

The empirical relationship developed by Glauert, including tip losses is:

$$a = (1/F)\left[0.143 + \sqrt{0.0203 - 0.6427(0.88 - C_T)}\right]$$

The Glauert empirical relationship is applicable when the axial induction factor a >0.4, or equivalently when the thrust coefficient CT <0.96. Although originally derived for the overall rotor thrust coefficient, it is commonly assumed to be valid for the local thrust coefficients at each blade section. These local values, denoted as CTr , represent the thrust contribution from individual annular sections of the rotor.

$$C_{T_r} = \frac{dT}{1/2\rho u_{\infty}^{2} 2\pi dr}$$

Recalling equation of the elemental thrust force from blade element theory, Then,

$$C_{Tr} = \sigma(1-a)^2 (C_L \cos\phi + C_D \sin\phi) / \sin^2\phi$$

Airfoil selection in HAWT Blade Design

The design of Horizontal Axis Wind Turbine (HAWT) blades relies heavily on understanding airfoil characteristics. A key factor affecting airfoil performance is the viscous nature of airflow, which is quantified using the Reynolds number. This dimensionless number reflects the ratio of inertial to viscous forces in the flow and is essential for predicting aerodynamic behavior under different conditions. The Reynolds number is defined by:

$$Re = \frac{u_{rel} c}{\upsilon}$$

Modern wind turbine airfoils vary in chord length—from around 0.3 meters on small turbines to over 2 meters on large, megawatt-scale rotors. With tip speeds between 45 and 90 m/s, the corresponding Reynolds numbers typically range from 0.5 million to 10 million, placing turbine airfoils in a flow regime where viscous effects are less dominant, but still important.

Because airfoil behavior changes significantly with Reynolds number, it's crucial to use data corresponding to the correct flow conditions during blade design. At low angles of attack - common in the windmill state of HAWTs - aspect-ratio effects are minimal, allowing the use of two-dimensional airfoil data. However, corrections like the tip-loss factor (as described in Equation 73) must be applied to account for threedimensional effects near blade tips.

Airfoil selection also involves meeting several engineering criteria, including aerodynamic performance, structural integrity, manufacturability, and maintenance considerations. A key aerodynamic parameter is the glide ratio, representing the balance between lift and drag forces, which is ideally high for efficient turbine operation. The glide ratio γ\gammaγ is defined by:

$$\gamma = \frac{C_D}{C_L}$$

HAWT airfoils are typically optimized for low angles of attack, where they provide high lift and low drag. In this study, the NACA 4412 airfoil was analyzed and added to the BLADE DESIGN program's airfoil database as a reference example.

Blade Design procedure

To design an optimal blade shape using a known airfoil, it is essential to determine the chord length and twist distribution along the blade span. These parameters are tailored for a specific tip-speed ratio that maximizes the power coefficient CP of the rotor.

The overall power coefficient depends on several factors, including the relative wind angle ϕ, the local tipspeed ratio λr, the glide ratio CD/CL, and the tip-loss factor F, as shown in the power coefficient expression. To achieve maximum performance, each blade element's contribution must be optimized, meaning the elemental power coefficient should be maximized locally across the blade.

For an airfoil with a known minimum glide ratio, a direct relationship can be established between the relative wind angle and the local tip-speed ratio to determine the optimum relative wind angle ϕopt. This condition can be expressed as:

$$\phi_{opt} \rightarrow MAX \left\{ \begin{matrix} F \sin^2 \phi (\cos\phi - \lambda_r \sin\phi)(\sin\phi \\ + \lambda_r \cos\phi)[1 - (C_D / C_L)\cot\phi] \end{matrix} \right\}$$

When the optimum relative wind angle is plotted against the local tip-speed ratio for various glide ratios, it has been observed that the resulting relationship is largely independent of both the glide ratio and the tip-loss factor. This insight allows the previously defined condition to be simplified into a more general form that can be applied across a wide range of operating conditions.

This leads to a refined relationship that determines the optimum relative wind angle purely as a function of the local tip-speed ratio, expressed as:

$$\phi_{opt} \approx MAX \left\{ \sin^2 \phi (\cos\phi - \lambda_r \sin\phi)(\sin\phi + \lambda_r \cos\phi) \right\}$$

Therefore, a general relationship can be established between the optimum relative wind angle and the local tip-speed ratio, applicable to any airfoil type.

This is achieved by taking the partial derivative of the previously defined expression to identify the condition for maximum elemental power contribution.

This derivation results in a simplified and widely applicable formula, introduced as:

$$\frac{\partial}{\partial\phi} \left\{ \sin^2 \phi (\cos\phi - \lambda_r \sin\phi)(\sin\phi + \lambda_r \cos\phi) \right\}$$

After some algebra,

$$\varphi_{opt} = (2/3)\tan^{-1}(1/\lambda_r)$$

After determining the optimum relative wind angle for a given local tip-speed ratio, the next step is to apply the equations derived from blade-element momentum theory, with modifications to include the tip loss factor. These modified equations are key to defining the blade shape and calculating the maximum power coefficient for the selected airfoil type.

The blade design procedure begins by dividing the blade into N elements, allowing the calculation of the local tip-speed ratio for each element. This process is based on a specific formula derived from the theory mentioned earlier, which ensures a precise and optimized blade design.

$$\lambda_{r,i} = \lambda(r_i / R)$$

The optimum relative wind angle for each blade element is determined as:

$$\varphi_{opt,i} = (2/3)\tan^{-1}(1/\lambda_{r,i})$$

The tip loss factor for each blade element can be found as:

$$F_i = (2/\pi)\cos^{-1}\left[\exp\left[\frac{-(B/2)[1-(r_i/2)]}{(r_i/R)\sin\phi_{opt,i}}\right]\right]$$

The chord-length distribution can then be calculated for each blade element by:

$$c_i = \frac{8\pi r_i F_i \sin\phi_{opt,i}}{BC_{L,design}} \frac{(\cos\phi_{opt,i} - \lambda_{r,i}\sin\phi_{opt,i})}{(\sin\phi_{opt,i} + \lambda_{r,i}\cos\phi_{opt,i})}$$

where,

CL,design, is chosen such that the glide ratio is minimum at each blade element.

The solidity can be calculated as follows:

$$\sigma_i = \frac{Bc_i}{2\pi r_i}$$

The twist distribution can be determined from the following equation which can be easily derived from the velocity diagram shown in Figure 9 as:

$$\theta_i = \varphi_{opt,i} - \alpha_{design}$$

where,

α design, is again the design angle of attack at which CL design is obtained.

the power coefficient is determined using a sum approximating the integral in C_p equation in the tip – loss factor theory as:

$$C_P = \sum_{i=1}^{N} \left[\begin{array}{l} \left(\frac{8\Delta\lambda_r}{\lambda^2}\right) F_i \sin^2\phi_{opt,i}(\cos\phi_{opt,i} - \\ -\lambda_{r,i}\sin\phi_{opt,i})\ldots \\ (\sin\phi_{opt,i} + \lambda_{r,i}\cos\phi_{opt,i}) \\ \left[1-(C_D/C_L)\cot\phi_{opt,i}\right]\lambda_{r,i}^2 \end{array} \right]$$

In summary, once an airfoil type is selected and both the tip-speed ratio and blade length (or rotor radius) are defined, the optimum blade shape can be determined. Using this optimized design, the maximum power coefficient can be calculated, allowing for the estimation of the maximum extractable wind power at any given average wind speed.

The design process begins by estimating the rotor radius based on required power and wind speed. After selecting the tip-speed ratio, number of blades, and aerodynamic conditions for minimal drag-to-lift ratio, the blade is divided into elements. Each element's shape is then defined using optimum rotor theory.

3D correction of Snel et al.

Rotation causes an increase in lift coefficient due to the stall delay effect, also known as rotational augmentation or centrifugal pumping. To account for this, Snel, Houwink, and Bosschers developed the 3D correction method, which adjusts the lift coefficient to reflect these rotational influences on airfoil performance.

$$C_{l,rot} = C_{l,2D} + 3.1\left(\frac{\Omega_r}{V_{rel}}\right)^2\left(\frac{c}{r}\right)^2\left(C_{l,pot} - C_{l,2D}\right)$$

equivalently:

$$C_{l,rot} = C_{l,2D} + 3.1\left(\frac{\lambda_r^2}{1+\lambda_r^2}\right)\left(\frac{c}{r}\right)^2\left(C_{l,pot} - C_{l,2D}\right)$$

The corrected lift coefficient CL,rot accounts for the rotational effects on the airfoil. It is derived using the 2D lift coefficient CL,2D of the non-rotating airfoil and the potential lift coefficient CL,pot , which represents the ideal lift without rotational influences. The potential lift coefficient is calculated using the following expression:

$$C_{l,pot} = 2\pi\sin(\alpha - \alpha_0)$$

The rotational correction is applied up to 80% of the blade radius and for angles of attack up to 30°, with the correction gradually reduced to zero by 50° to reflect diminishing effects at high angles. This adjustment improves prediction accuracy of the lift coefficient, especially when combined with tip loss correction.

Liu and Janajreh (2012) demonstrated that incorporating this model yields accurate predictions of the power coefficient when compared to experimental results. For a broader evaluation, Breton (2008) compares multiple stall delay models. Additionally, for more complex flow conditions, skewed rotor corrections may also be necessary, as detailed in studies by Liu and Janajreh (2012) and Lindenburg (2003).

Chord length distribution:

The chord length plays a critical role in both the aerodynamic performance and structural stiffness of a wind turbine blade. Since the maximum airfoil thickness is expressed as a percentage of the chord, its value directly influences blade strength and lift characteristics. Various studies have proposed formulas for determining the chord distribution, with one widely referenced approach based on the Betz ideal blade for aerodynamic optimization.

An example of such a formula is provided by Hau (2006) and Schubel and Crossley (2012), and is expressed as:

$$C(r)_{opt} = \frac{2\pi r}{B}\frac{8}{9C_L}\frac{U_\infty}{U_{rel}}$$

In this formulation, U∞ represents the design freestream wind velocity, while the local resultant air velocity Urel is calculated using the vector sum of the axial and tangential components:

$$U_{rel} = \sqrt{U_\infty^2 + V_w^2}$$

where Vw is the local angular velocity of the blade element.

An alternative expression for this relationship, as well as a formula for the flow angle ϕ, is provided by Gundtoft (2009). These are known as the Betz formulas, which are based on the optimum axial induction factor a=1/3, and can be expressed as:

$$\phi = \tan^{-1} \frac{2}{3\lambda_r}$$

In addition to:

$$c = \frac{16\pi R}{9BC_{L_D} \dfrac{1}{\lambda \sqrt{\lambda_r^2 + \dfrac{4}{9}}}}$$

where, C_{LD} is the design lift coefficient.

A simplified formula for chord distribution, ignoring wake rotation effects, is provided by Manwell et al. (2009). This method offers a practical way to estimate blade geometry under idealized conditions is expressed by:

$$c = \frac{8\pi r}{BC_l} \left(\frac{\sin \phi}{3\lambda_r} \right)$$

For rotors with tip speed ratios between 6 and 9, and using airfoil sections with negligible drag and tip losses, Betz's momentum theory provides a good approximation for chord distribution. However, this method becomes less accurate at low tip speeds, with high drag airfoils, and near the blade hub. Blades designed for optimal power production have larger chord lengths and greater twist angles closer to the root. While this approach offers useful insights, it results in high costs and complex manufacturing, suggesting that alternative design methods might be more suitable near the blade root.

Maalawi (2011) developed an analytical formula for the theoretical optimum chord distribution based on Glauert's optimum conditions, offering an improved method for blade design to achieve ideal aerodynamic performance.

$$c = \frac{8\pi r F \sin \phi}{BC_L \left(\dfrac{\lambda_r + \tan \phi}{1 - \lambda_r \tan \phi} - C_D / C_L \right)}$$

Maalawi (2011) developed a formula that includes tip losses and drag, providing a more accurate representation of rotor performance compared to previous models that neglected drag. Kulunk (2011) presented a similar formula, but with drag omitted, which has been referenced by other authors like Kulunka and Yilmazb (2009) and Rathore and Ahmed (2012). This approach, as defined by these researchers, offers a foundation for understanding how drag affects rotor efficiency, leading to further refinements in rotor design and performance modeling.

$$c(r) = \frac{8\pi r F \sin \phi_{opt} \left(\cos \phi_{opt} - \lambda_r \sin \phi_{opt} \right)}{BC_{ld} \left(\sin \phi_{opt} + \lambda_r \cos \phi_{opt} \right)}$$

The optimum flow angle ϕ opt is determined by the method that maximizes the Cl/Cd ratio, selecting the design lift coefficient (C_L,d}) accordingly. Ingram (2011) employed a simplified version for chord distribution, using ideal blade theory and accompanying the flow angle calculation approach. This combination streamlines the design process for HAWT systems, optimizing aerodynamic performance as expressed in the methodology applied.

$$c(r) = \frac{8\pi r \cos \phi}{3B\lambda_r}$$

Burton et al. (2001) provided a direct method to calculate the linear distribution of the chord and twist angle, offering a streamlined approach for rotor blade design. This method, as expressed in their work, simplifies the process of determining optimal blade geometry for efficient wind turbine performance.

$$\frac{c}{R} = \frac{8}{9\lambda_{0.8}}\left(2 - \frac{\lambda}{\lambda_{0.8}}\right)\frac{2\pi}{C_l \lambda B} \qquad \phi = \tan^{-1}\left(\frac{\left(1 - \frac{1}{3}\right)}{1 + \frac{2}{3\lambda_r^2}}\frac{1}{\lambda_r}\right)$$

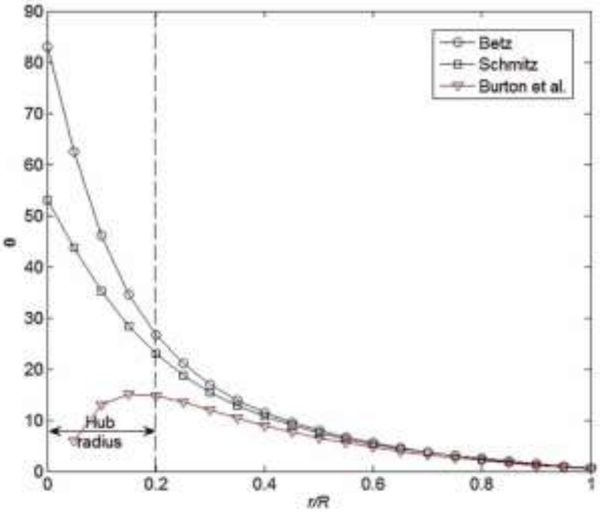

Figure 19: Flow angle calculated by Betz and Schmitz formulas for B = 3, λ = 5, α = 7° and CLD = 1.0

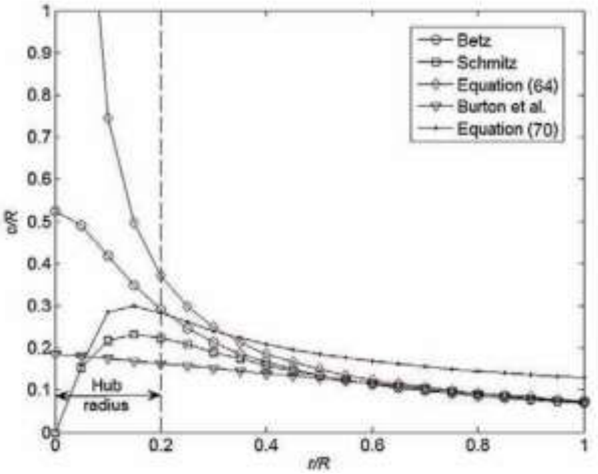

Figure 20: Comparison of chord distribution calculated by different methods for B = 3, λ = 5, α = 7° and CLD = 1.0

Rotor efficiency:

Rotor performance is often expressed using Froude efficiency, defined as the ratio of extracted power to available power. Originally used in marine engineering, this concept also applies to wind turbines to evaluate their efficiency on a unified scale.

$$\eta_{Froude} = \frac{Power\ extracted}{Power\ available} = \frac{Power}{\frac{1}{2}\rho U_\infty^3 A C_{p_{max}}}$$

$$\eta_{Froude} = \frac{C_p}{C_{p_{max}}} = \frac{C_p}{16/27}$$

Design methodology:

The aerodynamic design of rotor blades involves defining the chord and twist distributions along the blade span, based on predetermined values for power output, blade length, and tip-speed ratio. The process begins with selecting or estimating key design variables using expressions for the power coefficient C_p and the tipspeed ratio λ, as outlined below.

$$C_P = \frac{P}{\frac{1}{2}\rho U_\infty^3 \pi R^2}$$

$$\lambda = \frac{\Omega R}{U_\infty}$$

From the required power and angular speed, one can estimate the rotor radius by assuming an initial value for the power coefficient and knowing the site's wind conditions. Based on this, design values for tip-speed ratio and blade count are selected—typically three blades for ratios above 4. While increasing the tip-speed ratio can improve efficiency, excessively high values may cause aerodynamic interference between blades or structural stress, reducing performance or risking failure. Optimal performance is generally achieved at ratios between 6 and 7.

Table 1: Suggested blade number, for different tip speed ratios λ

λ	B
1	8–24
2	6–12
3	3–6
4	3–4
> 4	1–3

V.STRUCTURAL DESIGN

The structural design of Horizontal Axis Wind Turbines (HAWTs) ensures efficiency and durability under dynamic conditions. Key factors include fatigue analysis to assess resistance to cyclic stresses, damping to reduce vibrations, exergy analysis for thermodynamic efficiency, and twisting vibrations to maintain structural integrity. Together, these elements optimize the turbine's performance, longevity, and safety.

Figure 21: The coordinate definition of wind wheel

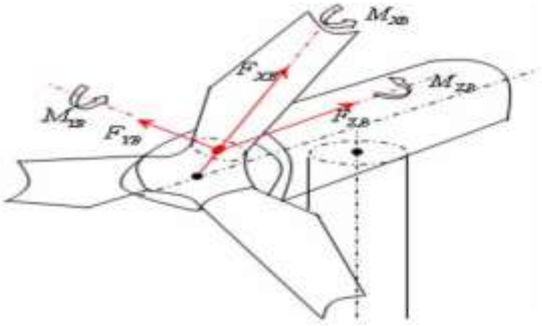

Fatigue Strength

Fatigue strength analysis is vital in wind turbine blade design, as blades face both deterministic and random loads. Material failure occurs when loads exceed the fatigue limit, with the S-N curve used to predict failure cycles, though it doesn't account for multistage loading. The fatigue life of blades is influenced by mechanical properties and load size, but assessing this life remains The key concepts and methods discussed include:

- **Stress - Time History σ(t)**

The fatigue analysis begins with obtaining the raw stress-time history, which is a time dependent variation of stress on the turbine blade:

σ(t) This can be measured directly using strain gauges or simulated using computational models like Finite Element Analysis (FEA).

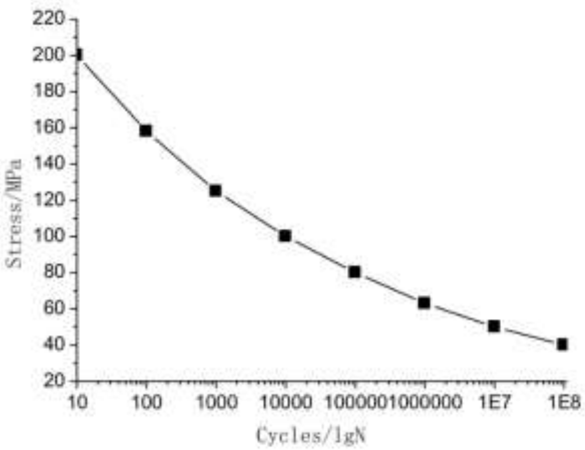

Figure 22: Fatigue feature curve of FRP material.
For example: Aeroblade1.5-40.3 wind turbine

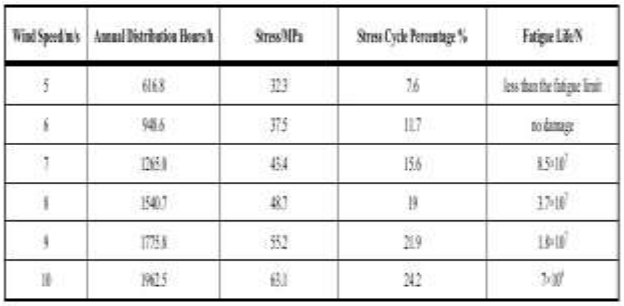

Wind Speed/m/s	Annual Distribution Hours/h	Stress/MPa	Stress Cycle Percentage %	Fatigue Life/N
5	616.8	32.3	7.6	less than the fatigue limit
6	948.6	37.5	11.7	no damage
7	1265.8	43.4	15.6	8.5×10^7
8	1540.7	48.7	19	3.7×10^7
9	1775.8	55.2	21.9	1.8×10^7
10	1962.5	63.1	24.2	7×10^6

Table 2: Aeroblade1.5-40.3 wind turbine blade spectrum

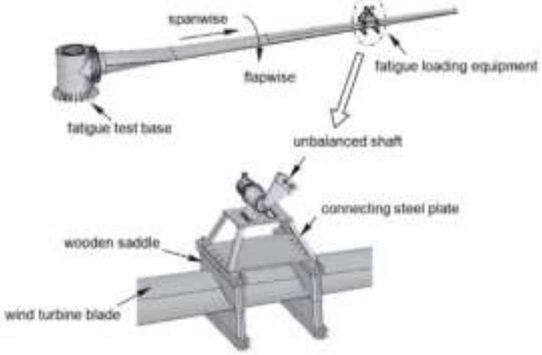

Figure 23: The structure of a single-point fatigue loading system for Aero blade

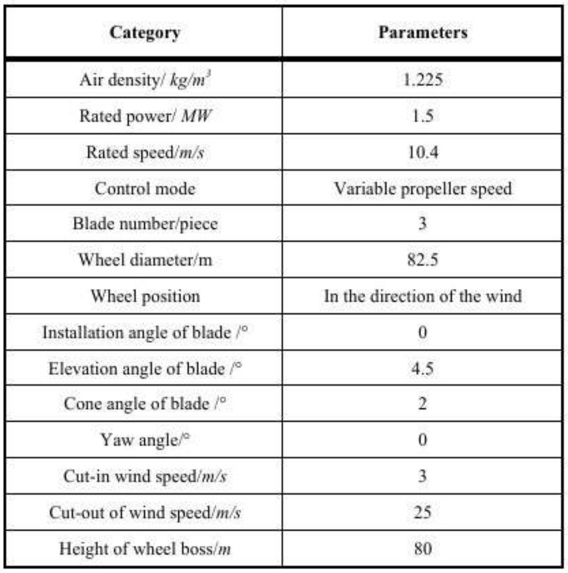

Category	Parameters
Air density/ kg/m^3	1.225
Rated power/ MW	1.5
Rated speed/m/s	10.4
Control mode	Variable propeller speed
Blade number/piece	3
Wheel diameter/m	82.5
Wheel position	In the direction of the wind
Installation angle of blade /°	0
Elevation angle of blade /°	4.5
Cone angle of blade /°	2
Yaw angle/°	0
Cut-in wind speed/m/s	3
Cut-out of wind speed/m/s	25
Height of wheel boss/m	80

Table 3: The basic parameters of Aeroblade1.5-40.3 wind turbine.

- **Moment Calculation:**

$$\sigma_b = \frac{My}{I}$$

σ_b – Bending stress

M – Calculated bending moment

y – Vertical distance away from the neutral axis

I – Moment of inertia around the neutral axis

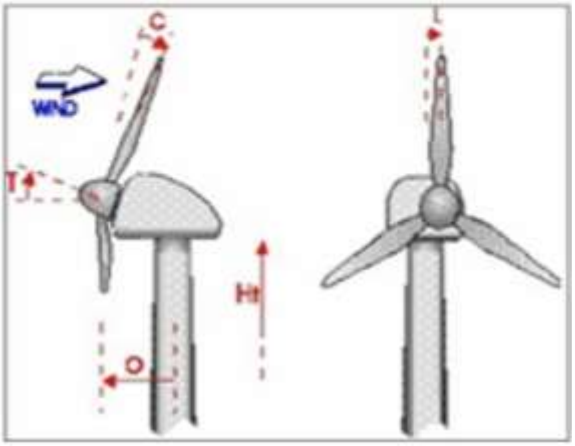

Figure 24: The bladed model of Aeroblade1.5-40.3 where,

T was elevation angle of blade; C was cone angle of blade; O was the suspension distance of wheel; L was lateral offset distance of blade; H was height of wheel boss.

Fatigue testing of wind turbine blades requires the bending moment error between calculated and measured values to remain within 7% along the blade span. The moment distribution is affected by the blade type and clump weight placement. To achieve accuracy, heavier clump weights should be placed near the blade root, with lighter weights towards the tip, following the predicted moment distribution. This ensures more accurate testing and minimizes errors.

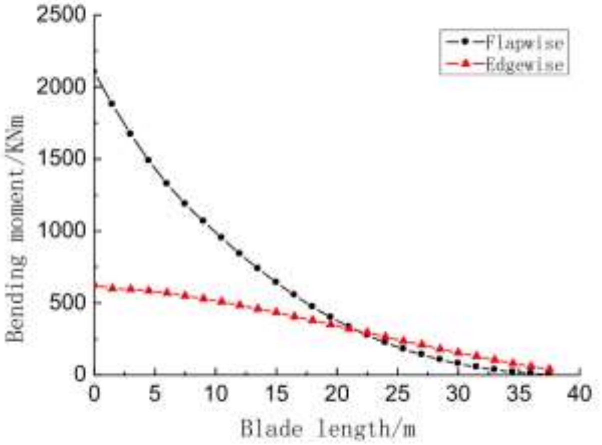

Figure 25: Moment distribute curve in flapwise and edgewise direction

- **Testing on Aeroblade1.5-40.3**

The Aeroblade1.5-40.3 blade was tested with fatigue loading equipment at 70% span, using a 250 kg eccentric mass and a 220 kg clump weight for moment matching. Blade amplitude was measured using a laser range meter, and the loading frequency was controlled at 0.78 Hz. The test simulated real-world conditions through multi-level amplitude loading and open-loop control.

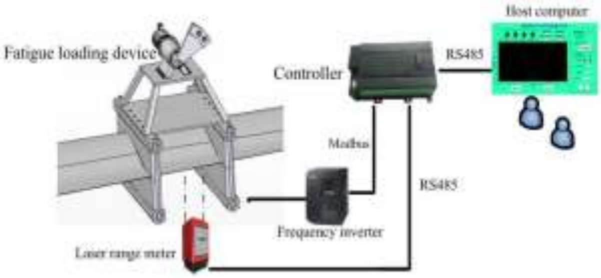

Figure 26: Control diagram

Figure 27: Aerobalde1.5-40.3 wind turbine blade fatigue loading test

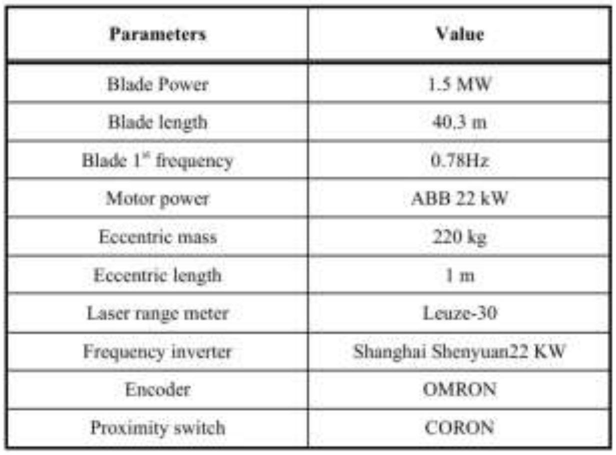

Parameters	Value
Blade Power	1.5 MW
Blade length	40.3 m
Blade 1^{st} frequency	0.78Hz
Motor power	ABB 22 kW
Eccentric mass	220 kg
Eccentric length	1 m
Laser range meter	Leuze-30
Frequency inverter	Shanghai Shenyuan22 KW
Encoder	OMRON
Proximity switch	CORON

Table 4: Test parametersTo shorten the fatigue loading test cycle and prevent the blades from experiencing the "exercise effect," a highlow loading sequence was used. The test involved 819,200 loading cycles. Due to the large amount of data, an Access database was utilized for efficient data storage and management. Vibration frequency and blade amplitude were recorded in real-time during the test.

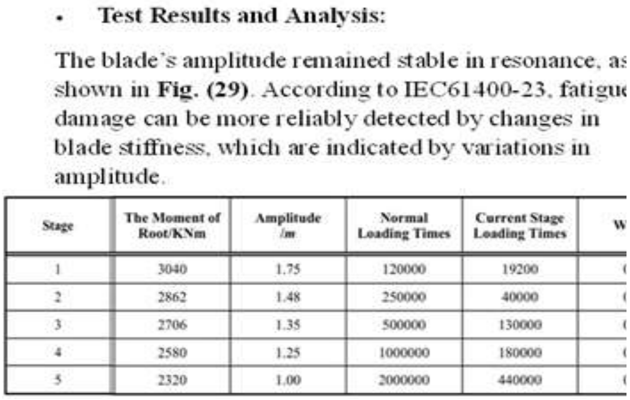

- **Test Results and Analysis:**

The blade's amplitude remained stable in resonance, a shown in **Fig. (29)**. According to IEC61400-23, fatigu damage can be more reliably detected by changes in blade stiffness, which are indicated by variations in amplitude.

Stage	The Moment of Root/KNm	Amplitude /m	Normal Loading Times	Current Stage Loading Times	W
1	3040	1.75	120000	19200	
2	2862	1.48	250000	40000	
3	2706	1.35	500000	130000	
4	2580	1.25	1000000	180000	
5	2320	1.00	2000000	440000	

Table 5: Fatigue loading outline

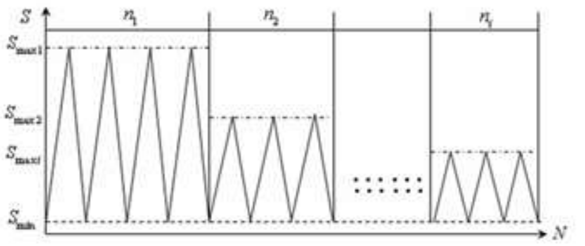

.

Figure 28: Aerobalde1.5-40.3 wind turbine blade high-low loading sequence

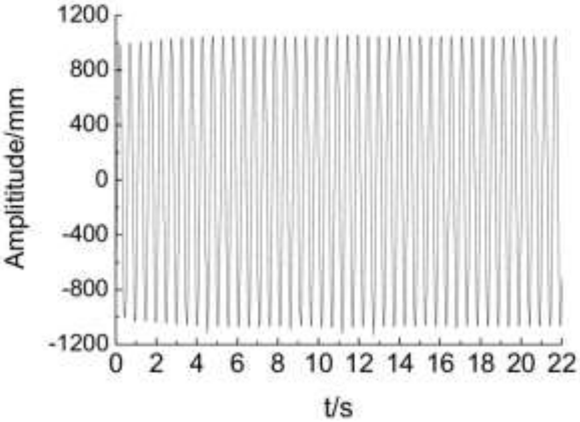

Figure 29: Wind turbine blade amplitude vary curve

After the game is finished, the same users are asked to fill out the post-game survey. This process helps

to evaluate the retention of concepts, improve Frequency statistics of the root's bending moment were performed, as shown in Fig. (10). The x-axis represents the ratio of the actual moment value to the set value. The results indicated that the loading point's amplitude remained stable due to the proper placement of the clump weight. The error in the bending moment. at the blade root did not exceed ± 0.4%.

- **Maximum and Minimum Stress**

The maximum stress σ_{max} and minimum stress σ_{min} are determined from the stress-time history, σ(t) as follows:

$$\sigma_{\mathrm{max}} = \max[\sigma(t)]$$
$$\sigma_{\mathrm{min}} = \min[\sigma(t)]$$

These two values represent the extremes of stress experienced by the turbine blade over its operational cycle.

- **Alternating Stress and Mean Stress**

With the maximum and minimum stresses determined, we calculate the alternating stress (σ_a) and mean stress (σ_m), which are important for fatigue life calculations.

- Alternating Stress (σ_a):

$$\sigma_a = \frac{(\sigma_{max} - \sigma_{min})}{2}$$

- Mean Stress (σ_m):

$$\sigma_m = \frac{(\sigma_{max} + \sigma_{min})}{2}$$

These quantities are crucial for assessing the cyclic loading conditions on the turbine blade.

- **Rain-flow Counting (Cycle Counting)**

The Rain-flow counting method is used to convert variable amplitude loading (i.e., non-sinusoidal stresstime data) into discrete cycles. This allows the calculation of fatigue damage more effectively for realworld stress histories, which typically have varying magnitudes over time. Rain-flow counting is typically implemented algorithmically, and no simple equation exists. However, this method ensures that each cycle (whether full or partial) is accounted for in the fatigue analysis.

- **Goodman Correction for Mean Stress**

The Goodman relation corrects the fatigue limit for the influence of mean stress and adjusts the alternating stress based on the mean stress level.

The Goodman relation is:

$$\frac{\sigma_a}{S_e} + \frac{\sigma_m}{S_{ut}} = 1$$

Where:

σ_a = alternating stress σ_m = mean stress

S_e = endurance limit (material property)

S_{ut} = ultimate tensile strength (material property)

The corrected alternating stress is calculated as:

$$\sigma_{a\_corrected} = (1 - \frac{\sigma_m}{S_{ut}})$$

This adjustment is necessary when the mean stress is large, as it significantly influences fatigue life.

- **High-Cycle Fatigue Life Estimation – Basquin's Law (S-N Curve)**

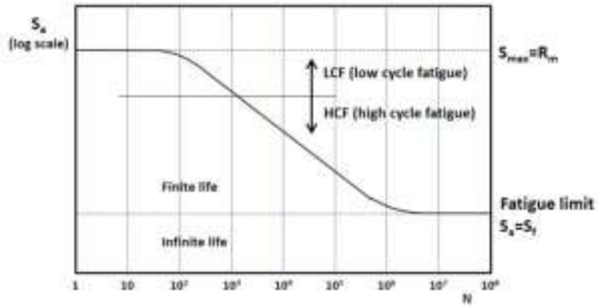

Figure 31: Basquin (S-N curve)

Basquin's equation, used for estimating fatigue life in the high-cycle fatigue regime, is expressed as:

$$\sigma_a = \sigma^{`}_f * (2N)^b$$

Where:

- σ_a = alternating stress
- σ'_f = fatigue strength coefficient
- b = fatigue strength exponent (material constant)
- N = number of cycles to failure (reversals)

Rearranged to solve for the number of cycles to failure:

$$N = (\frac{\sigma^{`}_f}{\sigma_a})^{\frac{1}{b}}$$

This equation is used to predict how many cycles a material can endure under a specific alternating stress.

- **Low-Cycle Fatigue – Morrow's Equation**

For low-cycle fatigue (LCF), where plastic deformation becomes significant, Morrow's equation is applied. This is particularly important for turbine blade roots, where large strains are observed. The equation is:

$$\varepsilon_a = \frac{\sigma_a}{E} + \varepsilon^{`}_f(2N)^c$$

Where:

εa = total strain amplitude E = Young's modulus

ε'_f = fatigue ductility coefficient
c = fatigue ductility exponent
N = number of cycles to failure (reversals)

Morrow's model is essential when large deformations are expected at certain regions of the blade.

- **Cumulative Damage – Miner's Rule**

The cumulative damage due to repeated loading is evaluated using Miner's Rule, which is used to calculate the total damage from different loading cycles. The equation is:

$$D = \sum \frac{ni}{Ni}$$

Where:

D = cumulative damage
ni = number of cycles at stress level i
Ni = number of cycles to failure at stress level i

Failure occurs when the cumulative damage D reaches 1.

- **Total Lifetime Prediction**

To estimate the total lifetime of the wind turbine blade, the cumulative damage is used to predict how long the blade will last under the given loading conditions.

$$\text{Life (years)} = \frac{1}{D_{\text{per year}}}$$

Where:

$D_{\text{per year}}$ is the cumulative damage per year.

<u>To sum up,</u>

Fatigue analysis for Horizontal Axis Wind Turbines (HAWTs) is a multi-step process involving stress-time history, cycle counting, alternating and mean stress calculation, and fatigue life prediction using models like Basquin's Law and Morrow's equation. Correcting for mean stress and using Miner's Rule for cumulative damage are essential steps for accurate fatigue life prediction. The S-N curve, Goodman diagram, and Morrow's curve are useful tools in this process, helping to understand the relationship between stress, cycles, and fatigue life under varying loading conditions. By using these methods, the longevity and reliability of wind turbine blades can be assessed, leading to safer and more efficient wind energy production.

- **Twist & Chord distribution**

The twist of a wind turbine blade is determined based on the orientation of the chord line and is closely related to the concept of pitch angle. This twist varies along the blade length to match the changing local airflow conditions. Near the root of the blade, where wind speeds are lower, the pitch angle is larger; towards the tip, where the blade moves faster, the pitch angle decreases. This variation is necessary because the apparent wind direction shifts along the blade due to increasing rotational speed from root to tip. To ensure each blade section maintains the most efficient angle of attack, the blade must be twisted accordingly.

The goal of this twist configuration is to maximize the lift coefficient at every point along the blade, as outlined by aerodynamic design principles. The chord direction— running from the leading edge to the trailing edge—is perpendicular to the blade's span. The point of maximum chord length is often referred to as the shoulder, while the tip has the smallest chord. Structurally, the root of the blade endures the highest stress, which is why it is also the thickest part. The thickness of the blade at various points is calculated as a percentage of the chord length at those locations. Typically, both the chord length and the blade thickness decrease progressively from the root to the tip, reflecting a design that balances aerodynamic performance with structural strength.

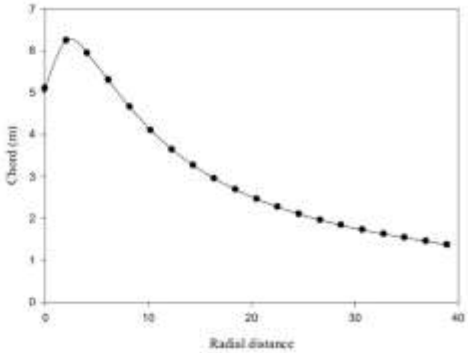

Figure 32: Chord distribution

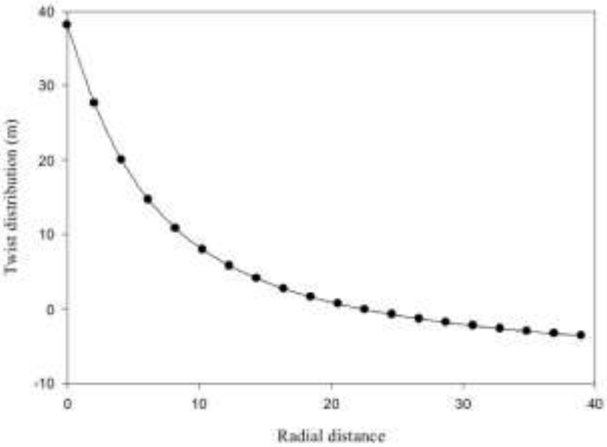

Figure 33: Twist distribution

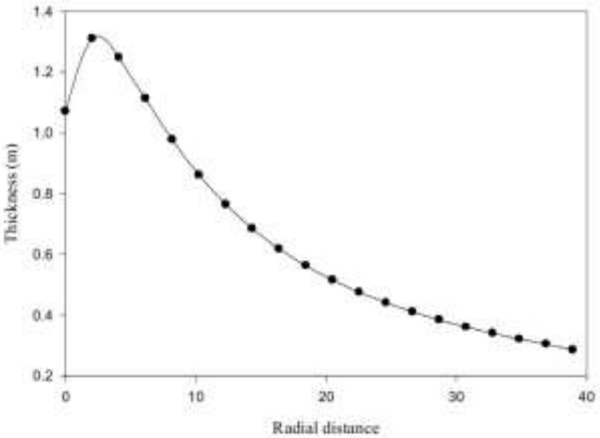

Figure 34: Thickness Distribution Chord and thickness peak near the root and taper toward the tip for strength and efficiency. Twist decreases along the blade to maintain optimal aerodynamic alignment with varying wind speeds.

Forces & Damping

- **Analysis of blade loading**

Rotating wind turbine blades experience varying loads over time, primarily due to aerodynamic forces, gravity, and centrifugal effects. To accurately analyze these forces and the resulting blade deflections, a specialized coordinate system is used. In this setup, one axis runs along the blade's length, another points horizontally toward the tower in the case of upwind turbines, and the third is oriented perpendicularly to both, forming a consistent right-handed system. This configuration remains valid regardless of the rotor's rotation direction or its position relative to the tower.

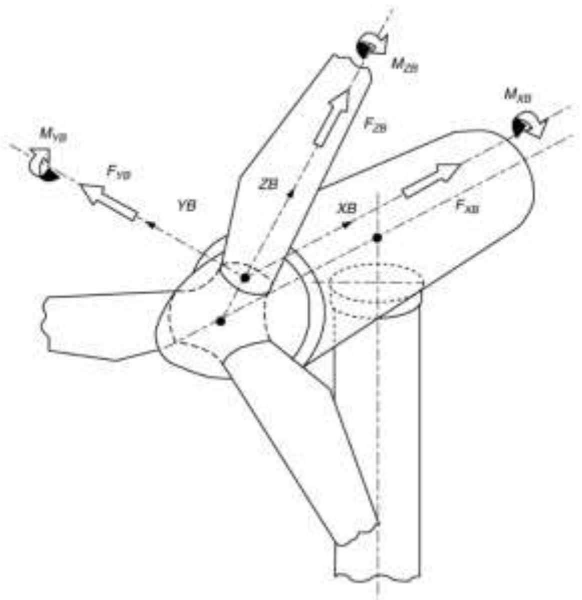

Figure 35: Coordinate system for blade loads and deflections

- **Aerodynamic damping**

Under steady wind conditions, aerodynamic forces on a wind turbine blade can be effectively analyzed using blade element–momentum theory. However, in unsteady or dynamic situations, factors like wind turbulence, yaw motion, and changes in rotational or pitch speed introduce additional complexities. These require consideration of dynamic inflow and stall effects to accurately capture the blade's aerodynamic behavior.

$$F_{XBa} = \frac{1}{2}\rho W^2 c(C_L \cos\varphi + C_D \sin\varphi)$$

$$F_{YBa} = -\frac{1}{2}\rho W^2 c(C_L \sin\varphi - C_D \cos\varphi)$$

Here, CL and CD represent the sectional lift and drag coefficients, W is the relative airflow velocity, ϕ is the inflow angle, ρ denotes air density, and c is the chord length at the section.

Momentum theory assumes an immediate response of the induced flow to changes in blade loading, but in reality, this adjustment takes time, a phenomenon known as "dynamic inflow."

Dynamic inflow, developed in helicopter aerodynamics, describes how the induced flow at the rotor depends on loading over time. The model used here, based on Pitt and Peters' work, avoids assumptions about inflow distribution by applying it at the blade element level.

Next, we will present the thrust coefficient equation, including dynamic inflow effects.

$$C_T = 4a(1-a) + \frac{8r}{\pi U}\dot{a}$$

Where, CT is the thrust coefficient, a is the axial flow induction factor, r is the radius of actuator annuli, U is the upstream wind velocity.

The last equation, as stated, replaces the blade element momentum theory for axial inflow, introducing a time lag that depends on radial position.

Dynamic stall, which influences aerodynamic loading, is accounted for by the Beddoes-Leishman model, given by indicial response functions and a time-lagged Kirchhoff formulation for trailing-edge separation.

The change in the normal force coefficient is split into non-circulatory and circulatory components. The next step is to derive the unsteady lift coefficient equation.

$$\Delta C_N^C = C_{N\alpha}\phi_\alpha^C \Delta\alpha$$

$$\Delta C_N^I = \frac{4}{M}\phi_\alpha^I \Delta\alpha$$

Where, CNα represents the slope of the normal force coefficient curve, M denotes the Mach number, ϕCα is the circulatory indicial function, and ϕIα is the noncirculatory indicial function.

In the Beddoes-Leishman model (B-L), the chordwise force coefficient is based on the circulatory component of the normal force coefficient. The attached flow response is calculated by superimposing individual indicial responses. This response is then modified by the position of the flow separation point, which reduces aerodynamic coefficients due to loss of circulation. The separation point is related to the normal force coefficient, given by:

$$C_N = C_{N\alpha}(\alpha - \alpha_0)\left(\frac{1+\sqrt{f}}{2}\right)^2$$

Where:

α: is the angle of attack.

α0: is the zero-lift angle of attack.

The static effective separation point is determined from static data and fitted to an exponential function. A firstorder lag is applied to account for the time delay in the movement of the separation point during unsteady conditions.

The model also includes vortex formation and shedding during dynamic stall, with vortex lift modeled as excess circulation near the airfoil. The increase in lift is based on the difference between the attached flow and the Kirchhoff equation's value. Time constants control the vortex growth, decay, and movement, with the vortex decaying exponentially as it reaches the trailing edge.

The lift and drag coefficients are calculated by resolving the normal and parallel components of the normal force and chordwise force, respectively, and adding the minimum drag.

$$C_L = C_N \cos\alpha + C_C \sin\alpha$$
$$C_D = C_N \sin\alpha - C_C \cos\alpha + C_{D0}$$

- Aerodynamic damping model

The tower is the vertical structure supporting the rotor and nacelle.

The aerodynamic damping model links tower top motion to changes in thrust. Wind disturbances alter inflow, affecting angle of attack and thrust. This change resists motion, providing damping.

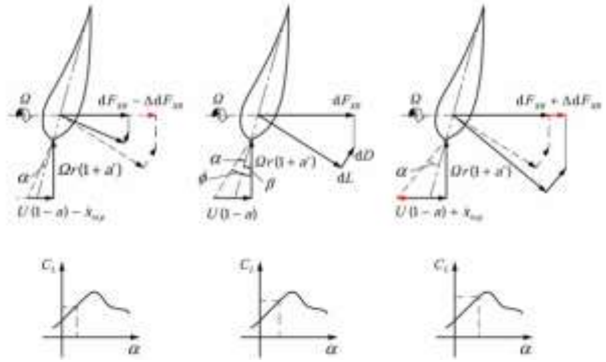

Figure 36: Tower Top Motion: 1. Along Wind Direction, 2. No Motion, 3. Against Wind Direction

In stall, damping may become negative, adding energy and risking self-excited vibrations. Lateral motion sees weaker damping. Assuming aligned wind and waves, the model shows aerodynamic damping helps reduce tower vibration and fatigue.

Aerodynamic damping arises from the interaction between the structural motion and rotor aerodynamics. A model can be developed by analyzing rotor aerodynamics with tower top motion included. This can be initiated by considering a wind turbine operating at constant speed. By examining the velocity components of an airfoil, the radial velocity Ur becomes:

$$U_r = \Omega r(1 + a')$$

and the downwind velocity:

$$U_d = U(1 - a) \pm \dot{x}_{top}$$

The equation can then be simplified as follows, given by:

$$\frac{\mathrm{d}F_{XB}}{\mathrm{d}r} = \frac{1}{2}\rho U_r^2 C_L c$$

Using the following assumptions:

- small inflow angle ϕ ($\cos\phi \approx 1$)
- high tip speed ratio ($U_r >> U_d$)
- attached flow ($C_L >> C_D$)

As (Ur≫Ud), the radial velocity is dominant,

$$\phi \approx \frac{U_d}{U_r}$$

A constant-speed horizontal-axis wind turbine (HAWT) yields:

$$\mathrm{d}\phi \approx \frac{\mathrm{d}U_d}{U_r}$$

The slope of the lift coefficient can be expressed as:

$$C_L' = \mathrm{d}C_l/\mathrm{d}\alpha$$

Since the inflow angle ϕ=α+β and the twist angle β is constant, it follows that:

$$\mathrm{d}C_L = C_L'\mathrm{d}\phi = C_L'\frac{\mathrm{d}U_d}{U_r}$$

Differentiate:

$$\mathrm{d}\left(\frac{\mathrm{d}F_{XB}}{\mathrm{d}r}\right) = \frac{1}{2}\rho U_r^2 c\,\mathrm{d}C_L = \frac{1}{2}\rho U_r c C_L'\mathrm{d}U_d$$

Since the apparent axial wind speed Ud is influenced by both changes in the wind speed and the structural motion, Then,

$$\mathrm{d}U_d = u - \dot{x}$$

u is the change in wind speed and x is the structural velocity (positive with the wind).

Re-writing the differentiated equation:

$$T' = \mathrm{d}\left(\frac{\mathrm{d}F_{XB}}{\mathrm{d}r}\right) = \frac{1}{2}\rho U_r c C_L'(u - \dot{x})$$

For a 1-degree of freedom mass-spring system, and applying the equation of motion:

$$m\ddot{x} + \frac{1}{2}\rho U_r c C_L'\dot{x} + Kx = \frac{1}{2}\rho U_r c C_L' u$$

Applying for damping per unit length:

$$\frac{\mathrm{d}c_a}{\mathrm{d}r} = \frac{1}{2}\rho U_r c C_L'$$

Integrate:

$$c_a = \frac{B\rho\Omega}{2}\int_{R_0}^{R} C_L' c r\,\mathrm{d}r$$

Where:

R0 is the blade root radius, and R rotor radius.

So, the aerodynamic damping ratio for the nth mode:

$$\xi_n = \frac{c_a}{2M_n\omega_n} = \frac{B\rho\Omega}{4M_n\omega_n}\int_{R_0}^{R} C_L' c r\,\mathrm{d}r$$

Taking that:

- ✦ Mn is the nth modal mass of the tower.
- ✦ ωn is the nth natural frequency of the tower.

For a variable-speed HAWT, changes in wind speed cause variations in rotor speed, requiring a new equation to replace the previous one, so:

$$\mathrm{d}\phi = \mathrm{d}\left(\frac{U_d}{U_r}\right)$$

Adding b as a correction factor allows for accounting for the gradual change in rotor speed in the simplified derivation.

$$\mathrm{d}\phi = b\frac{\mathrm{d}U_d}{U_r}$$

Then:

$$\xi_n = \frac{B\rho\Omega}{4M_n\omega_n}\int_{R_0}^{R} C_L{}'bcr\mathrm{d}r$$

✦ Quantitative findings (Numerically)

A power production load scenario is simulated for the HAWT under a turbulent wind field, featuring an average wind speed of 12 m/s and a longitudinal turbulence intensity of 19.6%. The variation in longitudinal wind speed at the hub height is illustrated in Fig. 38.

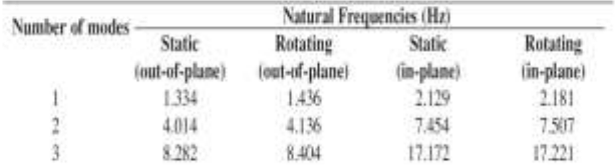

Number of modes	Natural Frequencies (Hz)			
	Static (out-of-plane)	Rotating (out-of-plane)	Static (in-plane)	Rotating (in-plane)
1	1.334	1.436	2.129	2.181
2	4.014	4.136	7.454	7.507
3	8.282	8.404	17.172	17.221

Table 6: Natural frequencies of the blade

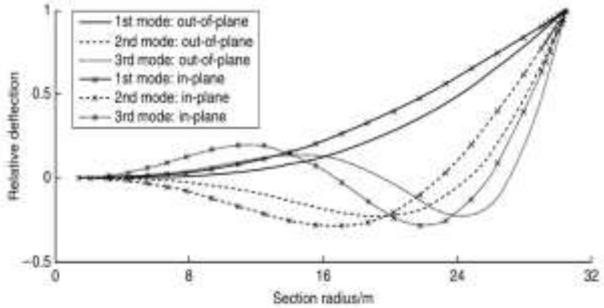

Figure 37: The former 3 mode shapes of the blade in out-of-plane and in- plane directions.

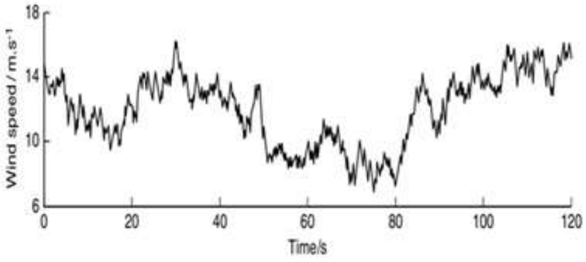

Figure 38: Longitudinal wind speed at hub center

In this simulation, the blade sections experience unsteady variations in angle of attack due to wind fluctuations and pitch control. Under dynamic stall conditions, the lift and drag coefficients no longer change uniformly with angle of attack, leading to a timedependent aerodynamic damping distribution along the blade. As the wind speed fluctuates around rated conditions, most blade sections remain outside the stall region, resulting in a generally positive aerodynamic damping effect that helps suppress blade vibrations. The analysis shows that aerodynamic damping is more significant in the out-of-plane direction compared to the in-plane direction, indicating a stronger influence on structural response in that direction for a HAWT.

- **Gravity Loads**

The blade continuously experiences gravitational loading, with the force components along each axis of the blade load coordinate system varying periodically with blade azimuth θ. When the shaft tilt angle χ and rotor coning angle β are taken into account, the gravitational force per unit length along each axis can be determined, given that:

$$F_{XBg} = \bar{m}g\cos\theta\sin\beta\cos\chi$$
$$F_{YBg} = \bar{m}g\sin\theta\cos\chi$$
$$F_{ZBg} = \bar{m}g\cos\theta\cos\beta\cos\chi$$

Where, m is the mass per unit length of the blade, g is the gravitational acceleration.

$$a = \begin{cases} (k+1)^{-1}, & a \le a_c \\ \frac{1}{2}\left(2 + k(1-2a_c) - \sqrt{(k(1-2a_c)+2)^2 + 4(k \cdot a_c^2)} - 1\right), & a \ge a_c \end{cases}$$

- **Centrifugal Loads**

Centrifugal forces, produced by the blade's rotation, act along the span of the blade. When accounting for the rotor coning angle β, the resulting centrifugal tension per unit length of the blade can be described as:

$$F_{ZBc} = \bar{m}\Omega^2 r\cos\beta$$

and centrifugal shear force:

$$F_{XBc} = \bar{m}\Omega^2 r\sin\beta$$

Where, **Ω** is the rotational speed of the rotor.

By combining the aerodynamic, gravitational, and centrifugal forces, the total load per unit length acting on the blade can be expressed as:

$$F_{XB} = F_{XBa} + F_{XBg} + F_{XBc}$$
$$F_{YB} = F_{YBa} + F_{YBg}$$
$$F_{ZB} = F_{ZBg} + F_{ZBc}$$

Exergy Analysis

According to BEM theory, which combines blade element and momentum theories, the aerodynamic behavior of wind turbine blades can be analyzed under the assumptions of incompressible and axisymmetric flow. Originally introduced by Froude and later refined by Glauert, this method segments each blade into smaller elements and evaluates their performance using momentum conservation principles. As the turbine rotates, it generates a wake that reduces the incoming wind speed due to induced velocity effects. This phenomenon affects the wind speed before it reaches the blades, denoted as V1, which is defined by the following equation:

$$V_1 = V_0(1 - a)$$

And for a (Axial induction factor):

As,

$$k = \frac{4f \sin \phi^2}{\sigma'\left(c_l \cos(\phi) + c_d \sin(\phi)\right)}$$

And,

$$\sigma' = 3c/2\pi r$$

Where: k is an auxiliary function and ac = 0.3 is the separation point of the thrust coefficient in the high axial induction fac tor, Cl and Cd are the lift and drag coefficient.

the tip loss correction factor:

$$f = \frac{2}{\pi}\arccos\left(e^{-\left(\frac{3(R-r)}{2r\sin\phi}\right)}\right)$$

for the rotational speed,

$$a' = \frac{w_{i2}}{\Omega}$$

Where: wi2 is the tangential induced velocity at the plane just before the rotor and a′ is the tangential induction factor.

Defining angle of flow and angle of attack:

$$\phi = a\tan\left(\frac{V_0(1-a)}{r\Omega(1+a')}\right) \qquad \alpha = \phi - \beta \quad ,$$

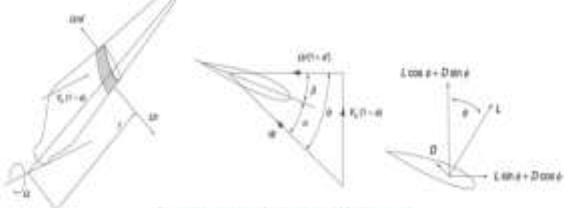

Figure 39: Arrangement of how to analyze the blade element

Referring to **Fig. 39**, to determine the power generated by a wind turbine, it is essential to evaluate both the axial and tangential components of the forces acting on each blade element. In this context, **V0** represents the free-stream wind speed, **Ω** is the angular velocity of the rotor, and rrr indicates the radial position of the blade element. The relative wind velocity at the element is denoted as **W**, while **β** and **ϕ** correspond to the blade pitch angle and the flow angle, respectively. The aerodynamic forces per unit length - lift **L** and drag **D** - are induced by the airflow around the blade and play a crucial role in calculating these force components.

$$W = \sqrt{V_0^2(1-a)^2 + \Omega^2 r^2 (1+a')^2}$$

$$L = \frac{1}{2}\rho W^2 C_l c, \quad C_l = f(r, \alpha)$$

$$D = \frac{1}{2}\rho W^2 C_d c, \quad C_d = g(r, \alpha)$$

$$dF_{ax} = L \cdot \cos(\phi) + D \cdot \sin(\phi)$$

$$dF_{tan} = L \cdot \sin(\phi) - D \cdot \cos(\phi)$$

$$\text{Power} = \Omega \int_{r_{hub}}^{R} dF_{tan} r dr$$

Tip speed ratio of the rotor**:**

$$\text{TSR} = \frac{\Omega R}{V_o}$$

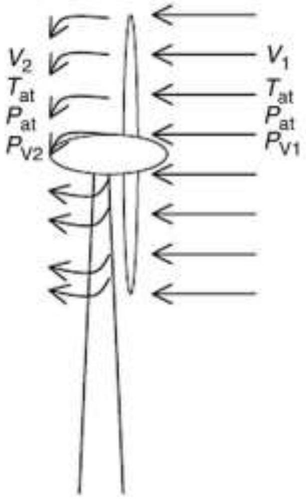

Figure 40: The diagram of inlet and outlet parameters energy passing through its cross-section per unit time, states in the rotor

Where: R is the tip radius

Exergy efficiency:

According to Betz's law, wind turbines are fundamentally limited to capturing less than 59% of the available wind energy. However, in real-world conditions, especially at higher wind speeds, their efficiency typically reaches around 40%. The overall energy efficiency is defined as the ratio of the useful mechanical power output to the change in kinetic energy of the incoming wind. In contrast, exergy efficiency considers the quality of energy and is calculated as the ratio of the useful work output to the total exergy of the wind stream passing through the turbine. The calculation of exergy efficiency is introduced next as given by:

$$\eta = \frac{W_{\text{out}}}{\text{kinetic energy of wind}}$$

$$\Psi = \frac{W_{\text{out}}}{\text{Ex}_{\text{flow}}}$$

Energy balance on wind turbine:

$$\text{ke}_1 = W_{\text{out}} + \text{ke}_2$$

Vibration Analysis

Vibration in Horizontal Axis Wind Turbines (HAWTs) refers to oscillations caused by aerodynamic forces, mechanical imbalances, and component interactions. Common sources include uneven wind loading, rotor imbalance, gearbox or generator faults, and tower-blade interactions. These vibrations can lead to structural fatigue, noise, and reduced efficiency. Monitoring systems are often used to detect and manage vibration, ensuring reliable and safe operation. The theoretical power in a cylindrical stream of air

T1,2 are calculated through the wind chill temperature:
Then, Exergy of humid air is:

$$\text{Ex}_{\text{flow}} = \text{Ex}_{\text{ph}} + \text{ke}$$

$$\text{Ex}_{\text{ph}} = m\left[c_{\text{p}}(T_2 - T_1) + T_0\left(C_{\text{P}} \ln\left(\frac{T_2}{T_1}\right) - R\ln\left(\frac{P_2}{P_1}\right) - \frac{C_{\text{P}}(T_0 - T_{\text{avg}})}{T_0}\right)\right]$$

Exergy balance on wind turbine:

$$v_2 = \sqrt[3]{\frac{2(\text{ke}_1 - W_{\text{out}})}{\rho\pi R^2 t}}$$

$$P = \frac{\mathrm{d}\left(\frac{1}{2}mV^2\right)}{\mathrm{d}t}$$

velocity is calculated by:

$$P = \frac{\mathrm{d}E}{\mathrm{d}t}$$

Where, E is the kinetic energy given by:

$$E = \frac{1}{2}mV^2$$

Angle of attack (degree)
0
2
4
6
8
10
12
14

$$\text{Ex}_{\text{ph}} = m\Big[(c_{p,a} + \omega c_{p,v})(T - T_0) - T_0\left[(c_{p,a} + \omega c_{p,v})\ln\left(\frac{T}{T_0}\right) - (R_a + \omega R_v)\ln\left(\frac{P}{P_0}\right)\right] + T_0\left[(R_a + \omega R_v)\ln\left(\frac{1 + 1.6078\omega_0}{1 + 1.6078\omega}\right) + 1 + 1.6078R_a\omega\ln\left(\frac{\omega}{\omega_0}\right)\right]\Big]$$

turbine's destruction can be defined by: For constant wind speed

$$\text{EX}_{\text{des}} = T_0\left(C_P\ln\left(\frac{T_2}{T_1}\right) - R\ln\left(\frac{P_2}{P_1}\right) - \frac{C_{\text{P}}(T_0 - T_{\text{avg}})}{T_0}\right)$$

Figure 41: Lift to drag ratio vs angle of attack

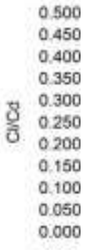

$$\frac{\mathrm{d}V}{\mathrm{d}t} = 0$$

Then:

$$P = \frac{1}{2}\dot{m}V^2$$

Mass flow rate:

$$\dot{m} = \rho AV$$

Where: cross-sectional area of the air column is A, and its density is ρ.

Substitute with $\boldsymbol{\dot{m}}$:

$$P=\frac{1}{2}\rho A V^3=\frac{1}{2}\rho\frac{\pi D^2}{4}V^3$$

As, D is air column diameter Conversely, the power extracted by the wind turbine from the airflow is given by:

$$P_T=T\omega$$

The wind turbine power coefficient:

$$C_p=\frac{T\omega}{\frac{1}{2}\rho A V^3}=\lambda C_m$$

Where: λ represents the tip speed ratio, defined as:

$$\lambda=\frac{\omega D}{2V}$$

The moment coefficient expressed by:

$$C_m=\frac{T}{\frac{1}{2}\rho A D V^2}$$

The equation of power coefficient will be used to assess wind turbine efficiency. The Betz limit sets the theoretical maximum power efficiency at 59%, but real turbines typically have power coefficients between 0.30 and 0.45 for large-scale turbines, with smaller turbines often being less efficient.

Rotating shafts may experience transverse oscillations, with centrifugal forces causing vibrations. These forces are described by the next equation:

$$F_c=M\omega^2\left(r+e\right)$$

Where: M represents the mass, r is the shaft deflection, (r + e) is the distance from the center of gravity, and ω denotes the angular velocity of the shaft. For the deflection force:

$$F=K_t r$$

$$K_t=M\omega_n^2$$ transverse stiffness

Equating Fc and F:

$$K_t r=M\omega^2\left(r+e\right)$$

After performing some algebraic simplification, the result is:

$$r=\frac{e}{\left(\frac{\omega_n}{\omega}\right)-1}$$

Where: ω_n is the shaft natural frequency.

When the shaft rotates at its natural frequency, vibrations increase, causing shaft to whirl. The natural frequency, representing oscillations without external interference, is given by:

$$f=\frac{\pi}{2}n^2\sqrt{\frac{gEI}{WL}}$$

Where: n is the mode, g is the constant of gravity, E is the young modulus, I is the moment of inertia, W is the shaft weight, and L is the shaft length.

Without damping, the dynamic response of the blade model can be described in matrix equation as:

$$KV=\omega^2 MV$$

Here, K is the stiffness matrix, M is the mass matrix, ω is the angular frequency of a vibration mode, and V is the mode vector defining the mode shape.

VI.VISUALIZATION DESIGN

The visualization phase focuses on developing a detailed and realistic model of the Horizontal Axis Wind Turbine (HAWT) to simulate its real-world structure and function. Creating an accurate visual representation is essential for understanding the geometry, assessing component interactions, and preparing for further stages such as simulation and prototyping.

A variety of computer-aided design (CAD) software options are available for 3D modeling, including Autodesk Inventor, CATIA, and Fusion 360. For this project, SolidWorks was selected due to its powerful design capabilities, ease of use, and strong support for mechanical assemblies. **Using SolidWorks**, each component of the wind turbine - such as the rotor blades, hub, nacelle, tower, and base - was individually modeled and then assembled into a complete system. The resulting model provides a clear, scalable, and editable design that closely reflects the intended real-world turbine.

Mechanical Assembly and Detailed Drawings

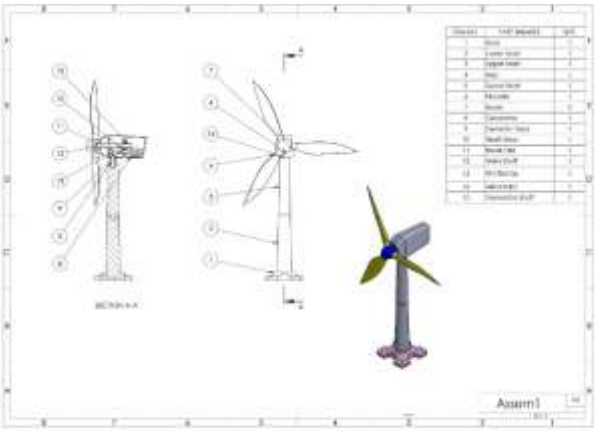

Figure 42: Assembly drawing for HAWT on SolidWorks

To access the detailed SolidWorks files for all parts, the full assembly, and technical drawings, you can click [here].

VII. RESULTS & DISCUSSION

Since the goal is to design a model that aligns with the required power and torque based on specific dimensions, various tools and software can be used to support this process. Examples include MATLAB, ANSYS, and QBlade, which allow for advanced simulation, optimization, and performance analysis. However, performing these simulations is beyond the current scope of our project. Instead, we focused on the theoretical foundation and searched for a relevant case study. We found a study conducted in Iran, where researchers applied the same theoretical equations we used. They utilized these advanced tools to link the equations with real performance parameters such as power and torque, successfully validating their design through simulation and practical analysis.

- South Khorasan Province (Iran) Fadashk station Case Study Results:

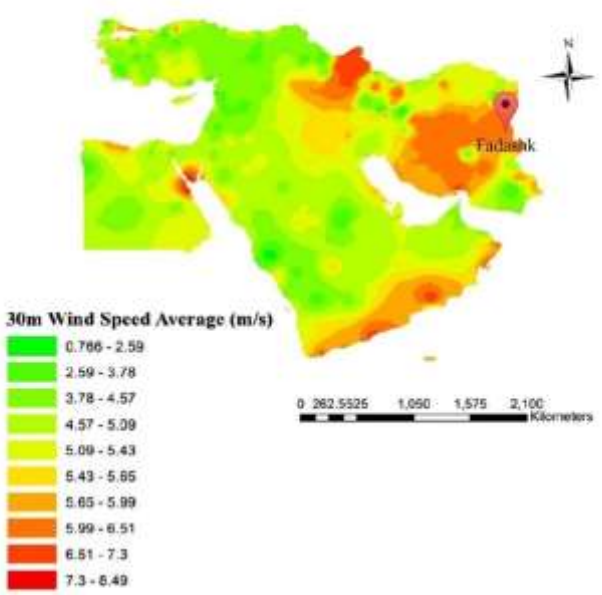

Figure 43: Average wind speed in Middle-East and parts of Africa and Europe at a height of 30 m

Wind data analysis commonly uses the Rayleigh and Weibull distributions. The Rayleigh distribution relies on the mean wind speed, while the Weibull distribution, with two parameters, better represents varied wind conditions. The Weibull distribution is used to determine regional wind characteristics.

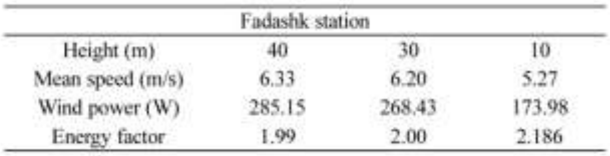

Fadashk station			
Height (m)	40	30	10
Mean speed (m/s)	6.33	6.20	5.27
Wind power (W)	285.15	268.43	173.98
Energy factor	1.99	2.00	2.186

Table 8: Calculation of parameters related to wind speed and power

Figure 44: Monthly mean speed distribution in the Fadashk station

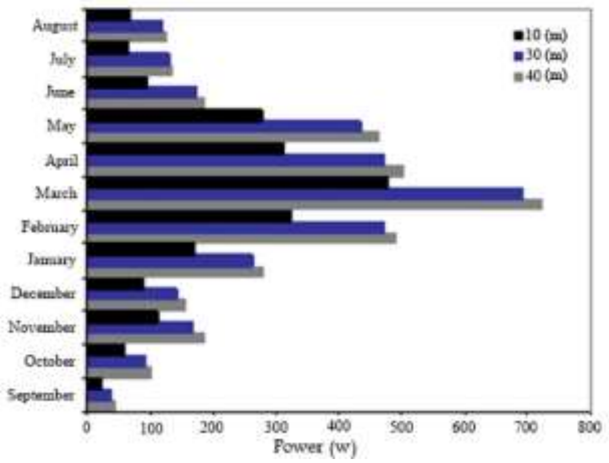

Figure 45: Monthly mean power variations in the Fadashk station

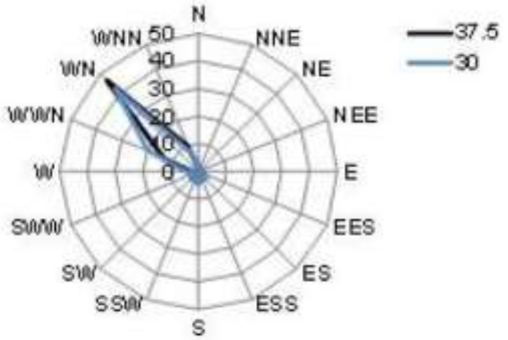

Figure 46: Wind rose diagram based on wind blow frequency in 37.5 and 30 m heights

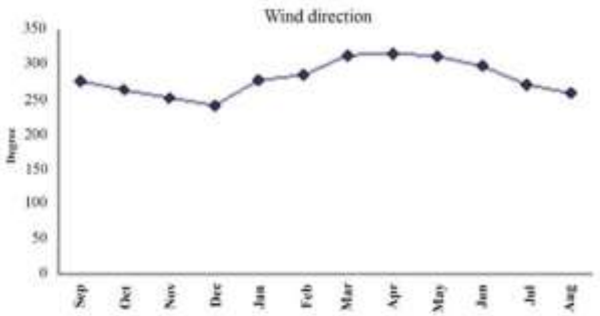

Figure 47: Distribution of the prevailing wind direction throughout the year in the Fadashk station

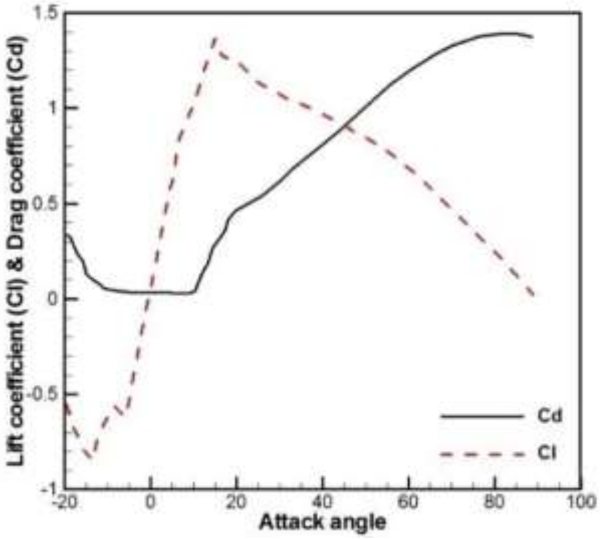

Figure 48: Lift and drag coefficients, C l and C d, respectively, for the S809 airfoil

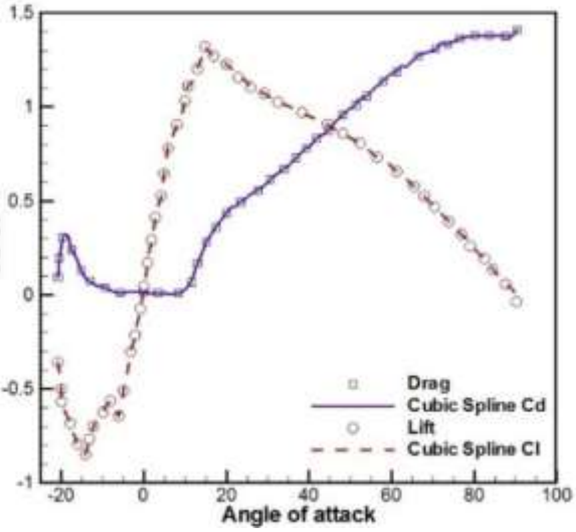

Figure 49: Curve fitting using Matlab software

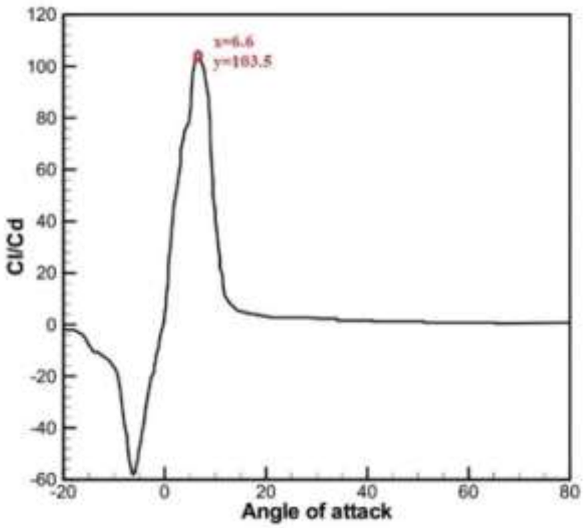

Figure 50: Cl/Cd versus the angle of attack (the most efficient angle of attack is shown by a circle)

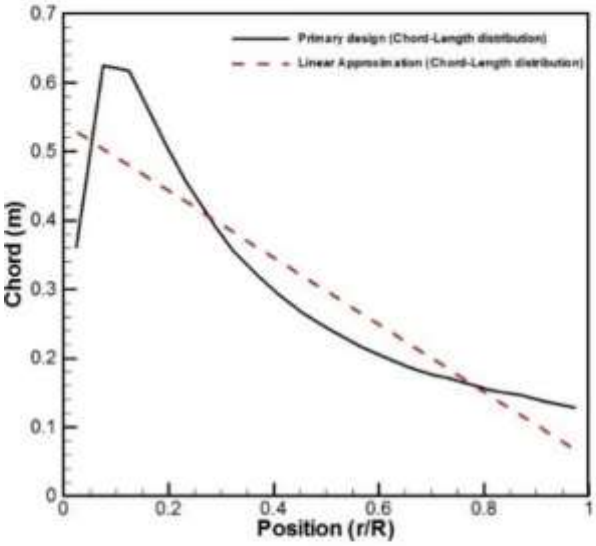

Figure 51: Chord-length distribution versus position

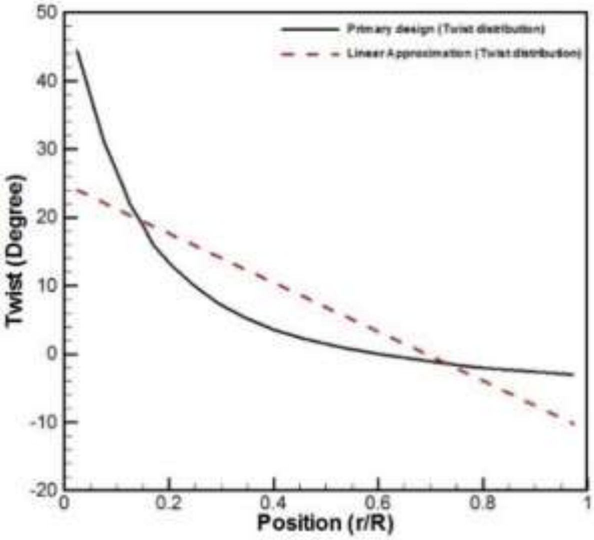

Figure 52: Twist distribution in the initial design

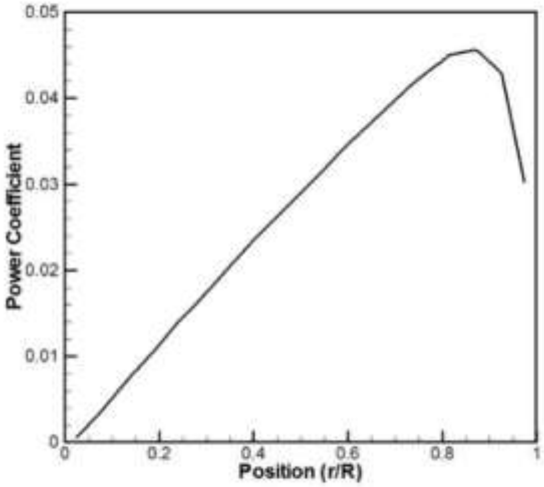

Figure 53: Power coefficient in the blade's length

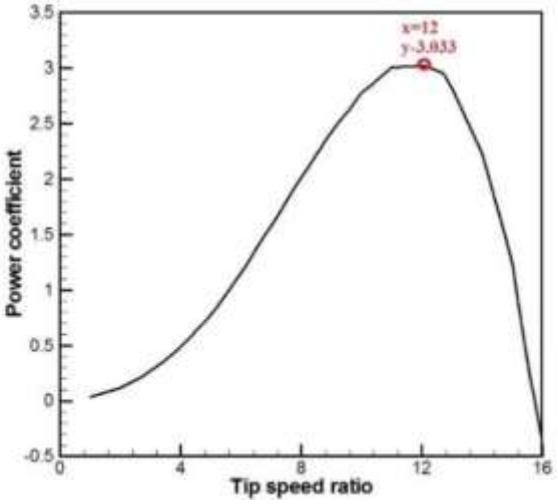

Figure 54: Cp-λ based on the first view

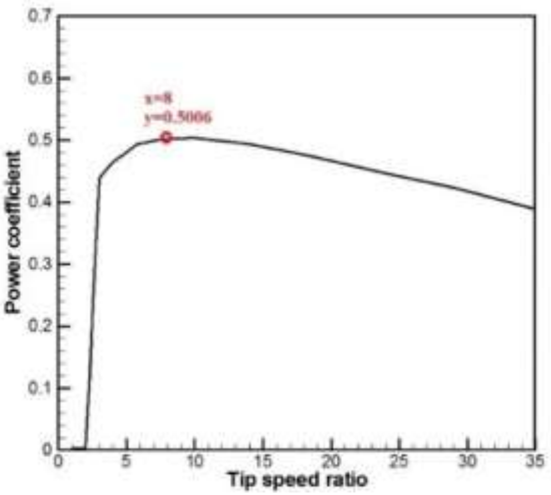

Figure 55: Cp-λ based on the second view

For a sample blade design case:

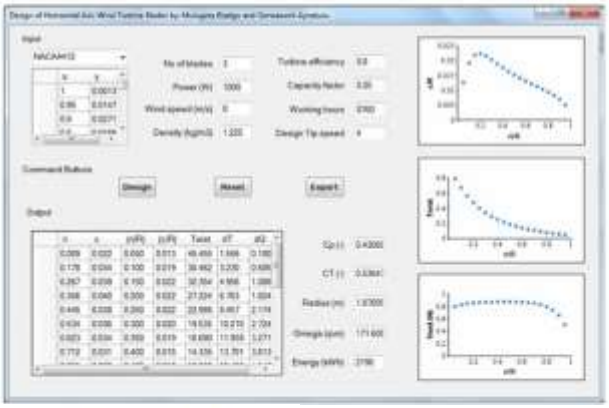

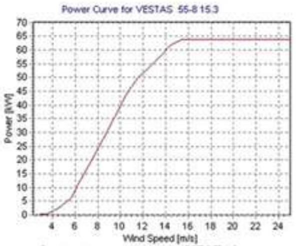

Company	VESTAS
Manufacturer	DK
Rated Power	55 kW
Small Generator	7.5 kW
Variable Speed	2 generator
Power control	Stall
Blade Type	ØKÆR
Rotor Diameter	15.3 m
Swept Area	184 m2
Power per m2	0.299 kW/m2
Rpm at rated power	50.4
Rpm at cut in	0 rpm
Standard hub height(s)	18 m
Tower	Lattice

r(m)	c (m)	Twist (deg.)	Trust (N)	Torque (Nm)
0.089	0.022	45.455	1.556	0.18
0.178	0.034	38.462	3.23	0.585
0.267	0.039	32.354	4.956	1.086
0.356	0.04	27.224	6.703	1.624
0.445	0.038	22.998	8.457	2.174
0.534	0.036	19.535	10.21	2.724
0.623	0.034	16.69	11.959	3.271
0.712	0.031	14.335	13.701	3.813
0.801	0.029	12.368	15.43	4.347
0.891	0.027	10.709	17.138	4.874
0.98	0.025	9.295	18.812	5.387
1.069	0.023	8.079	20.427	5.882
1.158	0.022	7.024	21.944	6.346
1.247	0.02	6.102	23.293	6.759
1.336	0.019	5.289	24.361	7.089
1.425	0.017	4.569	24.955	7.279
1.514	0.015	3.926	24.739	7.23
1.603	0.012	3.349	23.098	6.761
1.692	0.009	2.829	18.635	5.463

Table 10: Variation of blade chord, twist distribution, normal (thrust) force and torque along the blade

Figure 57 presents the normalized chord-length and twist distributions along the blade span for an optimum three-bladed rotor operating at a design tip-speed ratio of 4, using NACA4412 airfoil data at Re = 1×10^6. Table 1 lists these values numerically. The blade design output also includes key rotor parameters like radius, rotational speed, thrust, and power coefficients. Figure 58 provides an isometric view of the resulting blade elements.

Figure 58: Isometric views of the blade elements

VIII. CONCLUSION

This project provided a comprehensive analysis of rotor blade design for Horizontal Axis Wind Turbines, emphasizing the critical balance between aerodynamic performance, structural durability, and environmental adaptability. By applying Blade Element Momentum (BEM) theory, we successfully modeled the aerodynamic behavior of the blades under various wind speeds and pitch angles, enabling informed decisions about blade geometry and airfoil selection.

Meteorological factors such as air density, temperature, and pressure were incorporated into the aerodynamic and thermodynamic analyses to simulate realistic operating conditions. Exergy analysis further deepened our understanding of system performance by highlighting energy losses and irreversibilities that conventional efficiency metrics often overlook.

The stress analysis confirmed that the designed blade could endure fluctuating aerodynamic loads and dynamic forces without compromising structural integrity. Aerodynamic damping played a vital role in suppressing vibrations and enhancing the long-term stability of the rotor, especially for larger turbines exposed to significant aeroelastic effects.

Through the integration of simulation tools like CFD and SolidWorks, theoretical concepts were validated and translated into practical engineering outcomes. The insights gained from this study support the advancement of more reliable, efficient, and sustainable wind turbine technologies, reinforcing the global transition toward renewable energy solutions.

IX. RECOMMENDATIONS

This work presents a comprehensive design and preliminary validation of a horizontal axis wind turbine (HAWT) at a reduced scale, integrating theoretical modeling, aerodynamic blade design, and structural analysis using CAD tools and finite element methods. The study also encompasses key performance aspects, including exergy analysis and fatigue considerations, establishing a foundational model for future development.

To build upon the current study and further advance the design toward realistic performance evaluation and optimization, the following directions are recommended:

Advanced Aerodynamic Simulation

Future researchers are encouraged to conduct detailed computational fluid dynamics (CFD) simulations based on the current blade geometry. This will provide insights into flow behavior, pressure distribution, and aerodynamic efficiency under varying wind velocities and turbulence conditions.

Transient and Dynamic Load Analysis

It is advisable to perform dynamic simulations that account for fluctuating wind loads, including gusts and cyclic stresses. Modal and frequency analyses can help identify potential resonance issues and improve the structural robustness of the turbine under real-world operational scenarios.

Power Output Estimation

Using data obtained from CFD analysis, an estimation of the turbine’s electrical output should be conducted. Comparing these results with theoretical predictions will allow validation of design assumptions and provide a clearer picture of system performance.

Material Selection and Scaling Considerations

Further studies should explore alternative materials that offer improved strength-to-weight ratios and long-term durability, especially under fatigue loading. Considerations for full-scale implementation, manufacturability, and cost-efficiency should also be addressed.

Environmental and Exergy Efficiency Evaluation

Building on the initial exergy analysis presented in this study, a more detailed examination of the energy conversion efficiency and environmental impact over the lifecycle of the turbine is recommended. This would contribute to assessing the overall sustainability of the design.

Development of Control Strategies

As part of future development, the implementation of active control mechanisms—such as pitch and yaw regulation—can be investigated to optimize performance under varying wind directions and speeds. Integrating programmable controllers may enhance operational efficiency and adaptability.

REFERENCES

1. Global Wind Energy Council (GWEC), Global Wind Report Annual Market Update Statistics 2016, May 2017.
2. World Wind Energy Association (WWEA), World Wind Energy Report 2016, October 2016.
3. Rašuo, B., Dinulović, M., Veg, A., Grbović, A., Bengin, A.: Harmonization of new wind turbine rotor blades development process: A review, Renewable and Sustainable Energy Reviews, Volume 39, November 2014, pp. 874-882.
4. Manwell, J. F. and McGowan, J. G.: Wind energy explained: theory design and Application, John Wiley & Sons Ltd., 2009.
5. Wilson, R. E. et al.: Aerodynamic Performance of Wind Turbines. Energy Research and Development Administration, ERDA/NSF/04014-76/1, 1976.

6. Glauert, H.: Airplane Propellers, Aerodynamic Theory (W. F. Durand, ed.), Div. L, Chapter XI. Berlin, Springer Verlag, 1935.
7. Glauert, H.: The Elements of Aerofoil and Airscrew Theory. Cambridge University Press, Cambridge, UK, 1948.
8. Zhiquan, Y., Zhaoxue, C., Jingyi, C., Shibao, B.: Aerodynamic Optimum Design Procedure and Program for the Rotor of a Horizontal-Axis Wind Turbine, Journal of Wind Engineering and Industrial Aerodynamics, Vol.39, 1992.
9. Manwell, J. F., McGowan, J. G., Rogers, A. L.: Wind Energy Explained; Theory, Design and Application, John Wiley & Sons Ltd, 2002.
10. Spera, D. A.: Wind Turbine Technology, ASME Press, 1998.
11. Aagaard Madsen, H., Riziotis, V., Zahle, F., Hansen, M.O.L., Snel, H., Grasso, F., Larsen, T.J., Politis, E. and Rasmussen, F. (2012) ‘Blade element momentum modeling of inflow with shear in comparison with advanced model results’, Wind Energy, Vol. 15, No. 1, pp.63–81.
12. Buhl, M.L.J. (2005) A New Empirical Relationship between Thrust Coefficient and Induction Factor for the Turbulent Windmill State, NREL, USA.
13. Dixon, S.L. and Hall, C.A. (2010) Fluid Mechanics and Thermodynamics of Turbomachinery, 6th ed., Elsevier, New York.
14. Edon, M. (2007) Meter Wind Turbine Blade Design, June, Internship Report, Folkecenter for Renewable Energy.
15. Hansen, M.O. (2008) Aerodynamics of Wind Turbines, 2nd ed., Earthscan, UK and USA.
16. Lindenburg, C. (2003) Investigation into Rotor Blade Aerodynamics, Analysis of the Stationary Measurements on the UAE phase-VI Rotor in the NASA-Ames Wind Tunnel, ECN
17. Liu, S. and Janajreh, I. (2012) ‘Development and application of an improved blade element momentum method model on horizontal axis wind turbines’, International Journal of Energy and Environmental Engineering, Vol. 3, No. 1, R 10.1186/2251-6832-3-30
18. Marshall, L. and Buhl, J. (2005) A New Empirical Relationship between Thrust Coefficient and Induction Factor for the Turbulent Windmill State, Technical Report, August, NREL/TP-500-36834.
19. Montgomerie, B. (2004) ‘Methods for root effects, tip effects and extending the angle of attack range to 180 degree with application to aerodynamics for blades on wind turbines and propellers’, in FOIR1305, FOI, Swedish Defence Research Agency.
20. Raju, B.K. (2011) Design Optimization of a Wind Turbine Blade, Master thesis, The University of Texas at Arlington.
21. Tenguria, N., Mittal, N. and Ahmed, S. (2010) ‘Investigation of blade performance of horizontal axis wind turbine based on blade element momentum theory (BEMT) using NACA airfoils’, International Journal of Engineering, Science and Technology, Vol. 2, No. 12, pp.25–35.
22. J. Chen, and X. Wang, W. Shen, W. J. Zhu1, and N. S. Jens, “Optimization design of blade shapes for wind turbines,” Journal of Mechanical Engineering, vol.46, no.3, pp.131-134, 2010.
23. G. He, “Rotationnally sampled spectrum and fatigue life prediction of wind turbine system,” Journal of Harbin Institute of Technology, vol.42, no.5, pp.816-819, 2008.
24. C. W. Kensche, “Fatigue of composites for wind tuebines,” The 3rd International Conference on Fatigue of Composites, vol.9, pp.1-21, 2004.
25. A. Jorge, and V. Ale, “Aerodynamic loads and fatigue of small wind turbine blades standards and testing procedures,” Europe Wind Energy Event, vol.3, 2011.
26. Salzmann DJC, van der Tempel J. Aerodynamic damping in the design of support structures for offshore wind turbines. European Offshore Wind Conference. Copenhagen, Denmark2005.
27. Bonou A, Laurent A, Olsen SI. Life cycle assessment of onshore and offshore wind energy-from theory to application. Applied Energy. 2016.
28. Devriend C, Jordaens PJ, Sitter GD, Guillaume P. Damping estimation of an offshore wind turbine on a monopile foundation. EWEA 2012. Copenhagen, Denmark2012.
29. Rasmussen F, Petersen JT, Madsen HA. Dynamic Stall and Aerodynamic Damping. Journal of Solar Energy Engineering. 1999;121:150-5.
30. Leishman JG, Beddoes TS. A semi-empirical model for dynamic stall. Journal of American Helicopter Society. 1989.
31. Thomsen K, Petersen JT, Nim E, Øye S, Petersen B. A Method for Determination of Damping for Edgewise Blade Vibrations. Wind Energy. 2000.
32. Lu Ping, Qin Huifang, Luan Zhiyun. Dynamic analysis of tower structure for wind turbine based on finite element method. Chinese Journal of Mechanical Engineering, 2002.
33. Murtagh P J, Basu B, Broderick B M. Along-wind response of a wind turbine tower with blade coupling subjected rotationally sampled wind loading. Engineering Structures, 2005.
34. Younsi Rachid, El-Batanony Ismail, Tritsch J B, et al. Dynamic study of a wind turbine blade with horizontal axis. Wind Energy. 2001.

35. Kaushik SC, Singh OK. Estimation of chemical exergy of solid, liquid and gaseous fuels used in thermal power plants. J Therm Anal Calorim. 2014
36. Kalbasi R, Izadi F, Talebizadehsardari P. Improving performance of AHU using exhaust air potential by applying exergy analysis. J Therm Anal Calorim. 2020.
37. Namar MM, Jahanian O. Energy and exergy analysis of a hydrogen-fueled HCCI engine. J Therm Anal Calorim. 2019.
38. Koroneos C, Spachos T, Moussiopoulos N. Exergy analysis of renewable energy sources. Renew Energy. 2003.
39. Khosravi A, Koury RNN, Machado L, Pabon JJG. Energy, exergy and economic analysis of a hybrid renewable energy with hydrogen storage system. Energy. 2018.
40. Pope K, Dincer I, Naterer GF. Energy and exergy efficiency comparison of horizontal and vertical axis wind turbines. Renew Energy. 2010.
41. Bernabini L, Martinez J. An improved BEM model for the power curve prediction of stall-regulated wind turbines. Wind Energy. 2004.
42. Wang, T.G., Wang, L., Zhong, W., Xu, B.F. and Chen, L. (2012) Large-Scale Wind Turbine Blade Design and Aerodynamic Analysis. Chinese Science Bulletin Kexue Tongbao No. 5.
43. Murtagh, P.J., Ghosh, A., Basu, B. and Broderick, B.M. (2008) Passive Control of Wind Turbine Vibrations Including Blade/Tower Interaction and Rotationally Sampled Turbulence.
44. International journal of precision engineering and manufacturing vol. 18, no. 10, October 2017.
45. Jahangiri, M., Ghaderi, R., Haghani, A., and Nematollahi, O., “Finding the Best Locations for Establishment of Solar-Wind Power Stations in Middle-East Using GIS: A Review,” Renewable and Sustainable Energy Reviews, Vol. 66, pp. 38-52, 2016.
46. Burton, T., Jenkins, N., Sharpe, D., and Bossanyi, E., “Wind Energy Handbook,” John Wiley & Sons, 2001